Overview of the Spirit Mars Exploration Rover Mission to Gusev Crater: Landing site to Backstay Rock in the Columbia Hills

R. E. Arvidson,[1] S. W. Squyres,[2] R. C. Anderson,[3] J. F. Bell III,[2] D. Blaney,[3] J. Brückner,[4] N. A. Cabrol,[5] W. M. Calvin,[6] M. H. Carr,[7] P. R. Christensen,[8] B. C. Clark,[9] L. Crumpler,[10] D. J. Des Marais,[11] P. A. de Souza Jr.,[12] C. d'Uston,[13] T. Economou,[14] J. Farmer,[8] W. H. Farrand,[15] W. Folkner,[3] M. Golombek,[3] S. Gorevan,[16] J. A. Grant,[17] R. Greeley,[8] J. Grotzinger,[18] E. Guinness,[1] B. C. Hahn,[19] L. Haskin,[1] K. E. Herkenhoff,[20] J. A. Hurowitz,[19] S. Hviid,[21] J. R. Johnson,[20] G. Klingelhöfer,[22] A. H. Knoll,[23] G. Landis,[24] C. Leff,[3] M. Lemmon,[25] R. Li,[26] M. B. Madsen,[27] M. C. Malin,[28] S. M. McLennan,[19] H. Y. McSween,[29] D. W. Ming,[30] J. Moersch,[29] R. V. Morris,[30] T. Parker,[3] J. W. Rice Jr.,[8] L. Richter,[31] R. Rieder,[3] D. S. Rodionov,[22] C. Schröder,[22] M. Sims,[11] M. Smith,[32] P. Smith,[33] L. A. Soderblom,[20] R. Sullivan,[2] S. D. Thompson,[8] N. J. Tosca,[19] A. Wang,[1] H. Wänke,[4] J. Ward,[1] T. Wdowiak,[34] M. Wolff,[35] and A. Yen[3]

[1] Spirit landed on the floor of Gusev Crater and conducted initial operations on soil-covered, rock-strewn cratered plains underlain by olivine-bearing basalts. Plains surface rocks are covered by wind-blown dust and show evidence for surface enrichment of soluble species as vein and void-filling materials and coatings. The surface enrichment is the result of a minor amount of transport and deposition by aqueous processes. Layered granular deposits were discovered in the Columbia Hills, with outcrops that tend to dip conformably with the topography. The granular rocks are interpreted to be volcanic ash and/or impact ejecta deposits that have been modified by aqueous fluids during and/or after emplacement. Soils consist of basaltic deposits that are weakly cohesive, relatively poorly sorted, and covered by a veneer of wind-blown dust. The soils have been homogenized by wind transport over at least the several kilometer length scale traversed by the rover. Mobilization of soluble species has occurred within at least two soil deposits examined. The presence of monolayers of coarse sand on wind-blown bedforms,

[1]Department of Earth and Planetary Sciences, Washington University, St. Louis, Missouri, USA.

[2]Department of Astronomy, Space Sciences Building Cornell University, Ithaca, New York, USA.

[3]Jet Propulsion Laboratory, California Institute of Technology, Pasadena, California, USA.

[4]Max Planck Institut für Chemie, Kosmochemie, Mainz, Germany.

[5]NASA Ames/SETI Institute, Moffett Field, California, USA.

[6]Geological Sciences, University of Nevada, Reno, Reno, Nevada, USA.

[7]U.S. Geological Survey, Menlo Park, California, USA.

[8]Department of Geological Sciences, Arizona State University, Tempe, Arizona, USA.

[9]Lockheed Martin Corporation, Littleton, Colorado, USA.

[10]New Mexico Museum of Natural History and Science, Albuquerque, New Mexico, USA.

[11]NASA Ames Research Center, Moffett Field, California, USA.

[12]Companhia Vale do Rio Doce, Rio de Janeiro, Brazil.

[13]Centre d'Etude Spatiale des Rayonnements, Toulouse, France.

[14]Enrico Fermi Institute, University of Chicago, Chicago, Illinois, USA.

[15]Space Science Institute, Boulder, Colorado, USA.

[16]Honeybee Robotics, New York, New York, USA.

[17]Center for Earth and Planetary Studies, Smithsonian Institution, Washington, D. C., USA.

[18]Massachusetts Institute of Technology, Earth, Atmosphere and Planetary Science, Cambridge, Massachusetts, USA.

[19]Department of Geosciences, State University of New York, Stony Brook, New York, USA.

[20]U.S. Geological Survey, Flagstaff, Arizona, USA.

[21]Max Planck Institut für Sonnensystemforschung, Katlenburg-Lindau, Germany.

[22]Institut für Anorganische und Analytische Chemie, Johannes Gutenberg-Universität, Mainz, Germany.

[23]Botanical Museum, Harvard University, Cambridge, Massachusetts, USA.

[24]NASA Glenn Research Center, Cleveland, Ohio, USA.

[25]Department of Atmospheric Sciences, Texas A&M University, College Station, Texas, USA.

[26]Department of Civil and Environmental Engineering and Geodetic Science, Ohio State University, Columbus, Ohio, USA.

[27]Niels Bohr Institute, University of Copenhagen, Copenhagen, Denmark.

[28]Malin Space Science Systems, San Diego, California, USA.

[29]Department of Earth and Planetary Sciences, University of Tennessee, Knoxville, Tennessee, USA.

[30]NASA Johnson Space Center, Houston, Texas, USA.

[31]DLR Institute of Space Simulation, Cologne, Germany.

[32]NASA Goddard Space Flight Center, Greenbelt, Maryland, USA.

[33]Lunar and Planetary Laboratory, University of Arizona, Tucson, Arizona, USA.

[34]Department of Physics, University of Alabama at Birmingham, Birmingham, Alabama, USA.

[35]Space Science Institute, Martinez, Georgia, USA.

together with even spacing of granule-sized surface clasts, suggests that some of the soil surfaces encountered by Spirit have not been modified by wind for some time. On the other hand, dust deposits on the surface and rover deck have changed during the course of the mission. Detection of dust devils, monitoring of the dust opacity and lower boundary layer, and coordinated experiments with orbiters provided new insights into atmosphere-surface dynamics.

1. Introduction

[2] The Mars Exploration Rover, Spirit, touched down on the volcanic plains of Gusev Crater on 4 January 2004 at 04:35 UTC (Local True Solar Time (LTST) 14:25:09) at 14.571892 degrees south latitude and 175.47848 degrees east longitude, relative to the International Astronomical Union (IAU) 2000 body-centered coordinate frame [*Squyres et al.*, 2004a; *Arvidson et al.*, 2004a] (Figure 1). Spirit and her sister, Opportunity, are identical rovers equipped with the Athena Science Payload [*Squyres et al.*, 2003] (Table 1). The two rover missions have focused on use of remote sensing data to pick out important rock and soil targets and use of the rover's mobility system to traverse to the chosen targets to conduct detailed remote sensing and in situ observations. We note that soil is used in its planetary context and is meant to denote unconsolidated materials that can be distinguished from rock or bedrock. No implication is meant for the presence or absence of organic compounds. A prime focus of the rover missions has been to determine from measurements of the landforms, rocks, and soils the nature and extent to which water has interacted with surface and subsurface materials [*Squyres et al.*, 2004a, 2004b].

[3] The nominal mission for Spirit was scheduled for 90 Mars days or sols and results were reported in detail by *Squyres et al.* [2004a] and associated papers. In this paper we summarize major activities and scientific results associated with the first 512 sols of operations. Note that place names used in this paper for landforms, rocks, and soils encountered during Spirit's mission have not been approved by the International Astronomical Union and are meant to be informal and convenient ways to remember features (e.g., an outcrop or aeolian bedform) and targets (e.g., specific location on a feature for which in situ measurements were acquired). During the first 512 sols of operations, Spirit traversed from the plains landing site to the rim of the ∼210 m diameter Bonneville Crater, eastward across the plains, onto the West Spur of the Columbia Hills, across the saddle to Husband Hill, and up to the rocks and soils on the Cumberland Ridge on the northwest side of Husband Hill (Table 2; Figures 2 to 4). The transition from the plains to the Hills occurred after 157 sols of operations. Thus, for most of its lifetime the rover has been exploring and examining the terrains, rocks, and soils in the Columbia Hills. The mission has far exceeded its nominal 90 sol period (Figure 5, Tables 2–4). The rover as of sol 512 has traversed ∼4.4 km based on cumulative wheel turns and ∼3.9 km based on distances between image-based localization stations [*Li et al.*, 2006] (Figure 3).

[4] This overview paper is a lead-in to the many detailed papers describing scientific measurements and results for the Spirit mission, including papers that focus on each of the payload elements on the rover (Table 1) [*Bell et al.*, 2006; *Gellert et al.*, 2006; *Herkenhoff et al.*, 2006; G. Klingelhöfer et al., MIMOS II Mössbauer spectrometer investigation at Gusev Crater: From instrument characteristics through data analysis to the identification of olivine and goethite, manuscript in preparation, 2006 (hereinafter referred to as Klingelhöfer et al., manuscript in preparation, 2006)]. Papers are also included that focus on particular aspects of data from one or more instruments and that synthesize data across the various instruments and focus on the origin and evolution of the landforms, rocks, and soils [*Cabrol et al.*, 2006; *Farrand et al.*, 2006; *Fergason et al.*, 2006; *Golombek et al.*, 2006; *Grant et al.*, 2006; *Greeley et al.*, 2006; *Hurowitz et al.*, 2006; *Johnson et al.*, 2006; *McSween et al.*, 2006; *Ming et al.*, 2006; *Morris et al.*, 2006; *Squyres et al.*, 2006; *Wang et al.*, 2006a, 2006b; A. Knudson et al., Making tracks in Gusev crater: Mini-TES derived mineralogy of near-surface soils at the Mars Exploration Rover "Spirit" landing site, manuscript in preparation, 2006 (hereinafter referred to as Knudson et al., manuscript in preparation, 2006); S. W. Ruff et al., The rocks of Gusev crater as viewed by the Mini-TES instrument, manuscript in preparation, 2006 (hereinafter referred to as Ruff et al., manuscript in preparation, 2006); C. Schröder et al., Evidence for olivine weathering in rocks at Gusev crater, manuscript in preparation, 2006 (hereinafter referred to as Schröder et al., manuscript in preparation, 2006)]. Finally, a paper is included that summarizes use of bundle-adjustment techniques to delineate Spirit's locations as it traversed across the surface [*Li et al.*, 2006] and another that summarizes pipeline processing of data to use in operations [*Alexander et al.*, 2006].

2. Mission Operation Approaches

[5] The approach for operating both Spirit and Opportunity was defined before landing and was based on translating science objectives for the mission into specific tasks for the rovers to implement [*Squyres et al.*, 2003]. In addition, operational testing and rehearsals using the "FIDO" rover were conducted to prototype and refine operational concepts [*Arvidson et al.*, 2002]. During Spirit's mission each sol (Mars solar day, which is 24 hours, 39 minutes, 35 seconds in length) had a specific focus that typically centered on (1) remote sensing of the surface and atmosphere, (2) long drives, (3) approach drives to place the vehicle in a position so that the Instrument Deployment Device (IDD, see
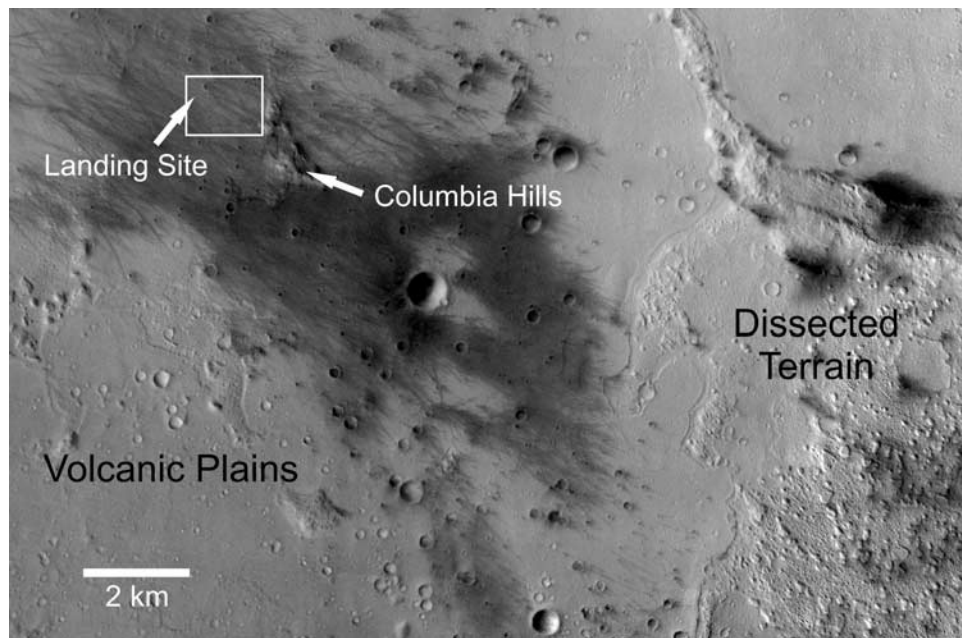
Figure 1. THEMIS-based mosaic showing the Spirit landing site in cratered plains in Gusev Crater. The Columbia Hills to the east of the landing site and the dissected terrain to the southeast are older deposits embayed by the plains materials. Dark streaks extending from plains craters are interpreted to be tracks of dust devils, where high winds eroded surface dust and exposed underlying materials. White box delineates area shown in detail in Figure 2. Frames V07909002 and V01580003, both acquired using band 3 (center wavelength of 0.654 micrometers). Former frame has a 67 degree solar incidence angle, and latter has a value of 51 degrees.

Table 1. Athena Payload and Engineering Camera Descriptions

| Instrument	Key Parameters
	Mast-Mounted
Pancam: Panoramic Camera	Twelve bands (0.4 to 1.0 μm) for stereoscopic imaging with 0.28 mrad IFOV; 16.8 deg by 16.8 deg FOV. Stereobaseline separation of 30 cm. External calibration target on rover deck.
MiniTES: Thermal Emission Spectrometer	Emission spectra (5 to 29 μm, 10 cm^{-1} resolution) with 8 or 20 mrad FOV. Internal and external blackbody calibration targets.
	IDD-Mounted In Situ Package
APXS: Alpha Particle X-Ray Spectrometer	^{244}Cm alpha particle sources, and x-ray detectors, 3.8 cm FOV.
MB: Mössbauer Spectrometer	^{57}Fe spectrometer in backscatter mode; Co/Rh source and Si-PIN diode detectors; field of view approximately 1.5 cm^2.
MI: Microscopic Imager	30 μm/pixel monochromatic imager (1024 $\times$ 1024) with 6 mm depth of field.
RAT: Rock Abrasion Tool	Tool capable of preparing 5 mm deep by 4.5 cm wide surface on rocks.
	Magnets
Filter	Located front of rover within Pancam FOV. Weak magnet to cull suspended particles from atmosphere and to be examined by MI, APXS, MB.
Capture	Located front of rover within Pancam FOV next to filter magnet. Strong magnet to cull suspended particles from atmosphere.
Sweep	Located next to Pancam calibration target. Intended to separate magnetic from nonmagnetic particles. To be examined by Pancam.
RAT	Four magnets of different strengths in RAT. To be examined by Pancam when IDD points RAT toward cameras.
	Engineering Cameras
Navigation Cameras (Navcam)	Mast-mounted panchromatic stereoscopic imaging system with 0.77 mrad IFOV; 45 deg FOV, and 20 cm stereobaseline separation. For planning sequences.
Hazard Avoidance Cameras (Hazcam)	Front and rear-looking panchromatic stereoscopic imaging systems with 2 mrad IFOV; 123 deg FOV, 10 cm stereobaseline separation. For path planning and hazard avoidance during traverses.
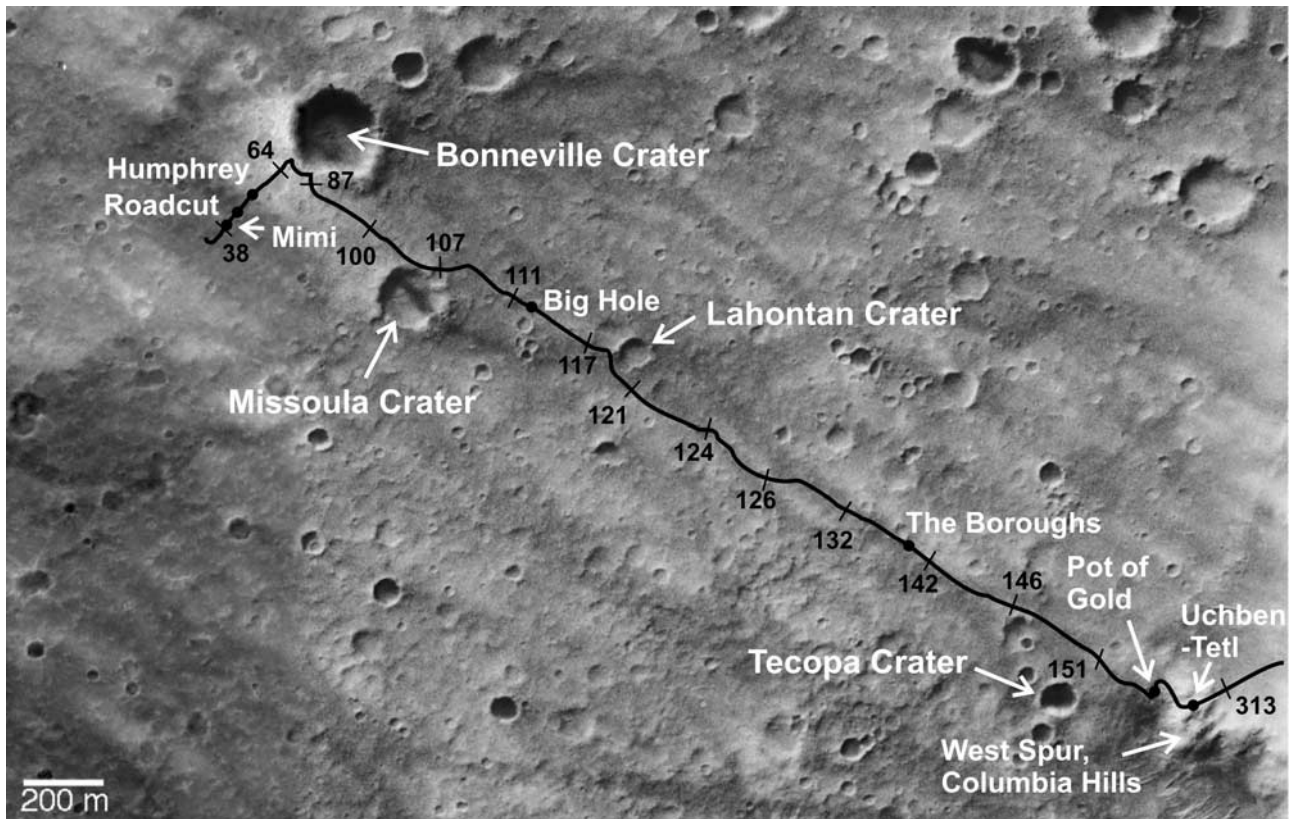
Figure 2. MOC Narrow Angle view of Spirit's traverses shown from the landing site to the west spur of Columbia Hills. Labeled with key features and events. Numbers represent rover locations on given sols. Mosaic of frames R1502643 and R2001024. Former has incidence angle of 33 degrees, and latter has 54 degrees.

Table 1) work volume included a designated rock or soil target, (4) deployment of the IDD for in situ work (use of the Rock Abrasion Tool (RAT) or measurements using the contact instruments (Table 1)), or (5) additional measurements for a given target using the IDD instruments, typically with a tool-change from one instrument to another (Table 2).

[6] Long drives included "blind" drive segments in which the rover was commanded to drive to a particular location without hazard avoidance systems activated. The distance for "blind" drives was governed by the extent to which potential hazards could be seen and avoided by Earth-based path planning in Pancam and Navcam images. In addition, auto-navigation was often used at the end of the "blind" drives to extend the total drive length. Auto-navigation driving was based on automated use by the vehicle of its Hazcam cameras (Table 1) to map the nearby terrain in stereo in the drive direction, generate topographic maps using the on-board computational system, and decide if obstacles needed to be avoided. When needed, the vehicle would drive around the obstacles while trying to go to a goal location defined by the engineering mobility team. In some cases when significant wheel slip was expected (e.g., on slopes) the rover would be commanded to acquire images of a given feature or features during the drive to update the rover's location relative to its goal point. This procedure was termed "visual odometry." Long drives would typically be followed by acquisition of 360 degree

Navcam panoramas for localization purposes and a series of Hazcam images to determine if the IDD could be safely deployed on a target of opportunity. In addition, a "touch and go" measurement was sometimes used before drives and focused on deploying the IDD during the morning on Mars for brief observations on a soil or rock target within the IDD work volume. These "touch and go" measurements were conducted until sol 297, when system lifetime issues dictated that the IDD be declared a consumable resource and its use became restricted to specific targets. Of course, each sol's plan typically included topical (e.g., images and MiniTES spectra of specific targets) and systematic (e.g., Pancam and MiniTES observations of the near-field) remote sensing observations of the surface and atmosphere, even for sols that involved long drives.

[7] As noted, approach sols focused on short drives or "bumps" to place a rock or soil target within the IDD work volume. Typically, Microscopic Imager (MI) data would be acquired on the next sol, followed by overnight Alpha Particle X-Ray Spectrometer (APXS), and Mössbauer Spectrometer (MB) observations (Tables 1 and 2). For important rock targets the RAT would then be used to brush dust and other loose material from rock surfaces, or to grind or abrade into the rock to depths of several millimeters before repeating the MI, APXS, and MB observations on newly exposed surfaces (Tables 2 and 3).

[8] Another distinctive sol type focused on implementation of soil properties experiments, including excavating
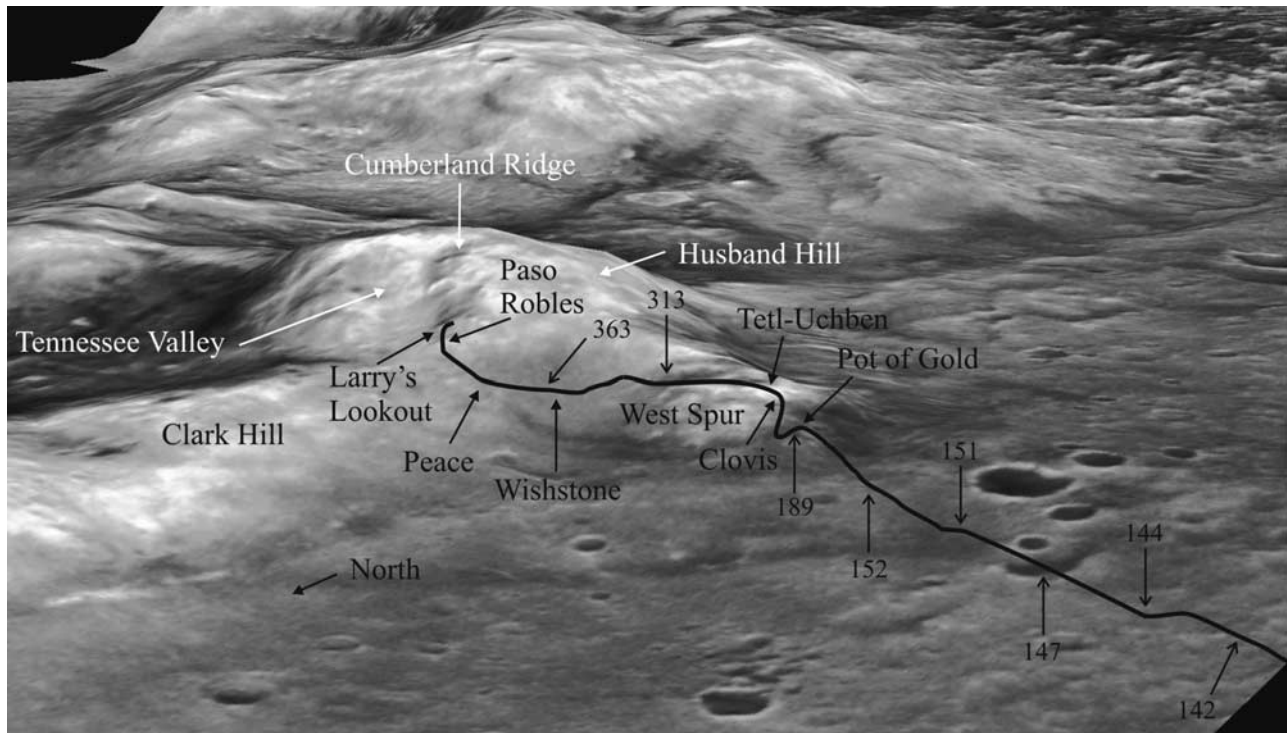
Figure 3. Perspective view of Columbia Hills looking to the southeast with Spirit's traverses from the plains to the Hills shown. Key features and measurement campaigns are identified, along with the ground track of the rover. The Tennessee Valley is shown. Cumberland Ridge is located on the southwest side of Tennessee Valley and strikes northwest-southeast. Numbers along side the track show rover locations on specific sols. Generated from stereogrammetric reduction of MOC NA frames R0200357 and E0300012.

trenches by turning the front two wheels inward and rotating the vehicle back and forth [*Arvidson et al.*, 2004a] (Table 4). As the vehicle rotated, the excavating wheel was used to dislodge and move soil to the left or right side of the rover. The net effect was to excavate a ~10 cm deep trench with a long axis aligned with the front end of the rover. Three trenches were excavated during the first 470 sols of operations (Figures 4 and 5 and Table 4). Another experiment, termed a "wheel scuff," consisted of turning a front wheel to an azimuth of 90 degrees relative to the drive direction, rotating the wheel, and backing up the rover. The result was to produce a shallow depression in the soil to expose subsurface materials (Figure 5 and Table 4). In some cases soil deposits disturbed by the wheels during rover maneuvers were found to be within the work volume of the IDD and the newly exposed materials were examined as targets of opportunity. Soil exposed by the wheels also provided convenient targets for Pancam and MiniTES observations of deposits with the ubiquitous dust cover removed [*Bell et al.*, 2004; *Christensen et al.*, 2004; Knudson et al., manuscript in preparation, 2006].

[9] Coordinated experiments between Spirit and the three active orbiters (Mars Global Surveyor, Odyssey, and Mars Express Orbiter) took place on a number of occasions. For example, Spirit acquired Pancam and MiniTES observations of the sky and surface while the Mars Express OMEGA instrument (imaging spectrometer operating from 0.38 to 5.08 micrometers) observed the landing site and surroundings from orbit [*Arvidson et al.*, 2004b]. In fact, the ~4 km of traverses conducted by Spirit with associated acquisition of remote sensing and in situ observations (Table 2 and Figures 4 and 5) have provided an unprecedented set of data for "ground truth" calibration of orbital remote sensing data.

[10] Planning for a given sol for Spirit started as soon as data from the previous sol's observations were received on Earth through some combination of direct to Earth transmissions using the high gain antenna and use of the ultra high frequency antenna to relay data through the Mars Global Surveyor or Odyssey spacecraft. The Spirit Science Operations Working Group considered results from initial analyses of data and implications of the new findings on both long term strategies and near term objectives. New sequences were developed in close cooperation with the rover mobility team (for traversing and deployment of the IDD) that fit power, data volume, and time constraints for the upcoming sol. These plans were refined and validated during the course of the planning cycle, leading to sequences that were uploaded to the rover by the Mars morning of the sol for which plans were prepared. The science team worked on Mars time shifts for the first several months of the mission, moving to Earth time after they became very efficient in analyzing data and generating new plans.

3. Mission Narrative

[11] The nominal mission for Spirit extended from landing (i.e., sol 1) to sol 90 and the first extended mission extended from sol 91 to 180. As noted, this paper covers the
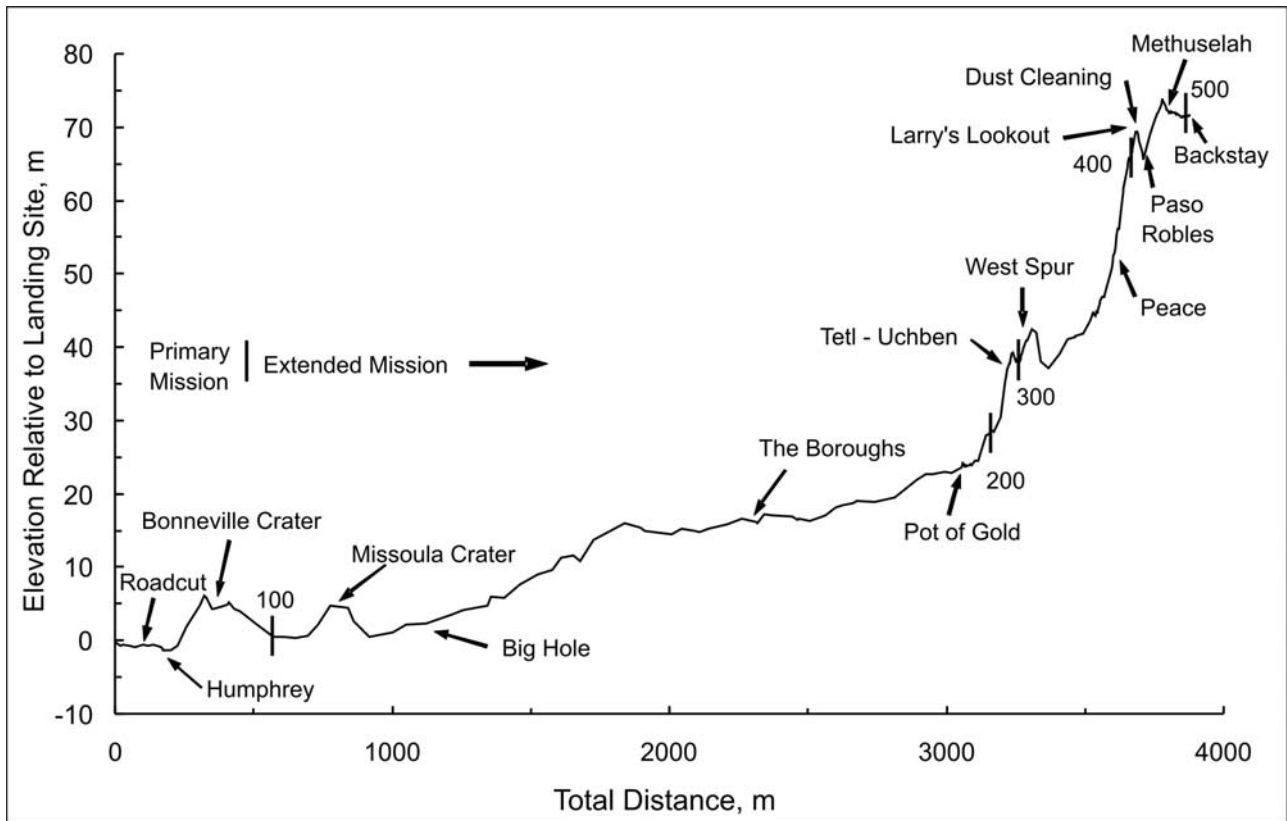
Figure 4. Traverse summary chart showing distance traveled (abscissa) versus relative elevation (ordinate), labeled with key features discussed in text. Sols associated with selected locations are also shown. Location data from *Li et al.* [2006].
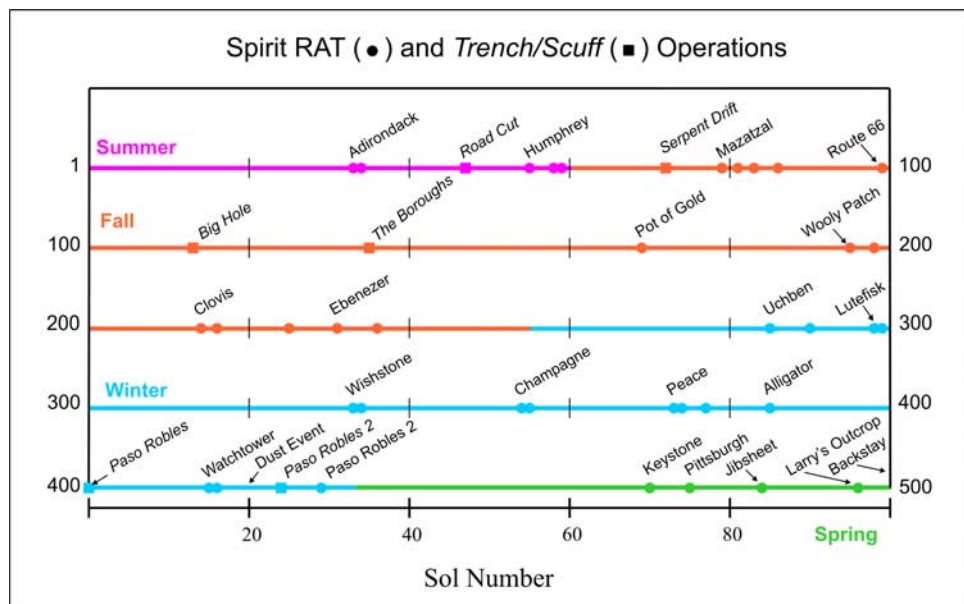

Figure 5. Timeline of RAT and soil trench and scuff operations, with southern hemisphere Martian seasons denoted. Road Cut is a trench in Laguna Hollow to the south of Bonneville Crater, Serpent Drift is the location of a soil scuff experiment near the rim of Bonneville Crater, Big Hole and The Boroughs are trenches on the plains, and Paso Robles is the site of bright soils exposed by wheel motions on Husband Hill. Pot of Gold was the first rock target on the West Spur of the Columbia Hills. The dust cleaning event refers to removal of soil from the solar panels by high winds. Remaining labels refer to RAT campaigns on rocks. Keystone and Pittsburgh are rock targets in the Methuselah outcrop.

Table 2. Major Activities for Spirit Organized by Sol[a]

Sols	Description of Activities	Site at Start of Sol
001–012	landing through egress; Mission Success Panorama	0
013–014	in situ observations of "First Pebble Flats" soil target; Mars Express Coordinated Experiment	3
015–017	Adirondack Drive, IDD, and RS	3
018–028	anomalies preclude science observations	3
029	Mars Express Coordinated Experiment	3
030–035	Adirondack IDD and RS	3
031–032	FLASH memory reformatting	3
036–040	White Boat, Stone Council Drives and RS; soil in situ measurements	3
038	anomalies preclude science observations	4
041–042	Mimi Approach, IDD, and RS; soil in situ measurements	5
043–044	soil in situ measurements; drive toward Bonneville Crater	7
045–046	soil in situ measurements; drive toward and RS of Laguna Hollow	9
047–050	Road Cut Trench Excavation, IDD, and RS	9
051–061	Humphrey Drive, IDD, and RS; soil in situ measurements; Legacy Panorama	11
061–071	Bonneville Crater Drive and RS; soil in situ measurements; Bonneville Panorama	12
072–074	Serpent Drift Trench, IDD, and RS	20
075–086	Mazatzal Drive, IDD, and RS; soil in situ measurements	22
085	sticky Mössbauer contact switch	22
087–089	drive toward Columbia Hills; soil in situ measurements	23
090–099	Route 66 Drive, IDD, and RS; software file upload	26
092–093	capture and filter magnets IDD observations	27
100–101	drive toward Columbia Hills	28
102	photometry and atmospheric measurements	29
103–112	drive toward Columbia Hills; soil in situ observations and RS	30
113–116	Big Hole Trench Excavation, IDD, and RS	37
117–134	drive toward Columbia Hills; soil in situ observations and RS	39
131–132	fix software error	51
135–142	The Boroughs Trench Excavation, IDD, and RS; Santa Anita Panorama	54
136–138	anomalies preclude science observations	54
143–156	drive toward Columbia Hills; soil in situ observations and RS	56
157	execution of onboard runout sequence	68
158–160	End of Rainbow Drive, IDD, and RS; soil in situ observations	68
161–172	Pot of Gold IDD and RS; soil in situ observations; Rover repositioning	69
173–182	Breadbox and String of Pearls IDD and RS; soil in situ observations and RS	69
176	calibrate front hazard avoidance camera	69
178	test visual odometry	69
183–185	wheel lube activity	70
186	IDD accuracy calibration	70
187–191	Loofah–Jeremiah IDD and RS; test drives	70
192–200	Wooly Patch Drive, IDD, and RS	75
201	failed drive due to excessive tilt angle	79
202–226	Clovis Drive, IDD, and RS; Cahokia Panorama	79
206–207, 224	anomaly precludes scientific observations	83
227–239	Ebenezer IDD and RS; soil in situ observations and RS	86
240	filter magnet in situ observations	88
241	communication errors, approaching conjunction	88
242–243	remote sensing	88
244–255	"no-op" commanding tests, conjunction	88
245–264	filter magnet and soil in situ observations and RS	88
262	anomaly precludes scientific observations	88
265	failed drive to "Tetl"	89
266–270	soil IDD and RS	89
271–276	Tetl Approach, IDD, and RS	89
277–278	anomaly precludes scientific observations	89
279–280	disturbed soil IDD and RS	89
281–295	Uchben Drive, IDD, and RS	89
296–303	Lutefisk Drive, IDD, and RS	89
304–306	drive toward Machu Picchu (Knoll on West Spur)	89
307–309	Magnet IDD and RS	90
310–313	drive east toward Husband Hill	90
313–317	soil scuff, IDD, and RS	92
317	drive toward Husband Hill	93
318–324	CCT and Capture Magnet IDD and RS; Thanksgiving Panorama	94
325–332	drive toward Husband Hill; Rover Deck Panorama	94
333–337	Wishstone IDD and RS	99
337–339	drive toward Husband Hill	99
339–346	rock stuck in wheel	101
340–349	soil IDD and RS	102
350–352	incomplete drives, soil in situ measurements and RS	102
353–358	Champagne IDD and RS	102
359	remote sensing	102
360–368	drive toward Larry's Lookout; RS	102
369–381	Peace Drive, IDD, and RS	102

Table 2. (continued)

Sols	Description of Activities	Site at Start of Sol
381–386	Alligator Drive, IDD, and RS	102
383–384	sequence uplink not received	102
386–398	drive toward Larry's Lookout; RS	102
395–397	flight software load	104
399–403	Paso Robles 1 IDD and RS; Phobos observations	105
399	drive failure	105
404–409	drive toward Larry's Lookout; RS	106
406	Phobos observations	107
408	unable to uplink plan due to a DSN transmitter failure	107
410–413	remote sensing; Larry's Lookout Panorama	108
414–419	Watchtower IDD and RS	108
419–431	Paso Robles 2 Drive, Scuff, IDD, and RS	108
431–444	drive, RS, and soil in situ observations	108
444	Odyssey into safe mode	109
445–448	Odyssey recovery; RS	109
449–453	remote sensing	109
454–456	drive and RS; Methuselah Panorama	109
456–461	Crumble Scuff, IDD, and RS	109
461–468	drive and Methuselah-targeted RS	109
469–476	Methuselah: Keystone and Pittsburgh IDD and RS; drive to additional targets	109
477–479	Liberty Bell Soil IDD	109
480–487	Jibsheet: Keel and Davis IDD and RS	109
488–503	Larry's Outcrop: Ahab, Moby, and Doubloon IDD and RS	109
504–506	IDD Magnet and Solar Cells; RS	109
507–512	Backstay Drive, IDD, and RS	109

[a]IDD, Instrument Deployment Device; RS, remote sensing.

period from landing to the second extended mission, up to and including sol 512. Covering operations and first-order science results through sol 512 is a logical and convenient ending point for this paper because by sol 512 the rover had traversed from the plains landing site onto the outcrops on the Cumberland Ridge on Husband Hill, an area rich in information about the landform and deposits that formed the Hills. The last rock examined on the Ridge was Backstay, a loose rock located to the south of the Methuselah and Jibsheet outcrops (Table 2 and Figures 4, 5, and 16).

[12] Soon after Spirit touched down and started acquisition of Pancam, Navcam, and Hazcam imaging data and MiniTES emission spectra it became apparent that the rover landed in dusty, soil-covered, rock-strewn cratered plains [*Squyres et al.*, 2004a; *Bell et al.*, 2004; *Christensen et al.*, 2004; *Grant et al.*, 2004]. Observations using the full payload soon showed that the rocks and soils were derived from olivine-bearing basaltic rocks [*Gellert et al.*, 2004; *Morris et al.*, 2004, 2006; *McSween et al.*, 2004, 2006]. These initial measurements were confirmed through detailed remote sensing and in situ measurements of the rocks Adirondack and Humphrey, including use of the RAT brush and grinding mechanisms to expose new surfaces, followed by acquisition of in situ measurements. In an attempt to sample strata from beneath the basaltic rocks, Spirit was commanded to traverse onto the ejecta deposits of the

Table 3. Summary of Major Rock Campaigns[a]

Name and RAT Operations	Brief Description
Plains	
Adirondack (brush and 2.7 mm grind)	Float near lander
Humphrey (brush and 2.1 mm grind)	Float on rim of hollow
Mazatzal (brush and two grinds 3.79 and 4.1 mm)	Float on Bonneville Crater ejecta
Route 66 (brush)	Float on Bonneville Crater ejecta
West Spur	
Pot of Gold (0.2 mm)	Float on rim of Hank's Hollow
Wooly Patch (two grinds: 5.17 mm Sabre and 4.02 mm Mastodon)	Outcrop or float
Clovis (8.89 mm grind)	Outcrop or float
Ebenezer (3.42 mm grind)	Float
Uchben (brush and 5.88 mm grind)	Outcrop or float
Lutefisk (brush)	Float
Husband Hill	
Wishstone (3.18 mm grind)	Float
Champagne (3.95 mm grind)	Float
Peace (two grinds: 3.22 and 9.7 mm)	Outcrop or float
Watchtower (6.48 mm grind)	Outcrop on Larry's Lookout
Keystone and Pittsburgh (brush)	Outcrop on Methuselah
Keel and Davis (brush)	Outcrop on Jibsheet
Paros, Ahab (brush), Doubloon, and Moby (brush)	Outcrop on Larry's Outcrop

[a]Grind or abrasion depths from S. Gorevan et al. (personal communication, 2005).

Table 4. Summary of Major Soil Campaigns

Name	Brief Description
Road Cut Trench	Exposed subsurface soils in Laguna Hollow ~100 m from lander
Serpent Drift Scuff	Scuff exposed subsurface soil in edge of drift near rim of Bonneville Crater
Big Hole Trench	Exposed subsurface soils in plains during transit to Columbia Hills
The Boroughs Trench	Exposed subsurface soils in plains during transit to Columbia Hills
Paso Robles Scuff	Scuff into bright, sulfur-rich soil on Husband Hill caused by wheel slippage during rover traverse

~210 m diameter Bonneville Crater, located several hundred meters to the northeast of the landing site (Figure 2). The intent was to search for material excavated by the Bonneville event from beneath the basaltic plains rocks, focusing on finding evidence for preplains aqueous processes. A search of the ejecta deposits and remote sensing of the interior of Bonneville Crater showed only basaltic rocks (including Mazatzal and Route 66) similar to those found on the plains [*Squyres et al.*, 2004a; *Bell et al.*, 2004; *Christensen et al.*, 2004; *McSween et al.*, 2004]. Thus the next phase of the extended mission focused on a rapid transit across the plains to the Columbia Hills (Figure 2). The reason is that the Hills are clearly embayed by the basaltic plains materials and thus are older than the materials at the landing site. The hope was that the Hills rocks contained evidence for aqueous processes associated with the early history of Gusev Crater. During the traverse to the Hills remote sensing and IDD-based measurements were conducted on a regular schedule [*Crumpler et al.*, 2005]. Spirit conducted remote sensing observations for several craters and associated ejecta deposits during its traverses across the plains, including the 163 m diameter Missoula crater, and the 90 m wide Lahontan crater [*Grant et al.*, 2006] (Figure 2). Two trenches were excavated during the plains transit to characterize subsurface soils (Big Hole and The Boroughs, Figure 2 and Tables 2 and 4). Once the West Spur of the Columbia Hills was reached on sol 157 and initial measurements were made it became clear that Hills rocks have been extensively modified by aqueous processes. The objective then focused on ascending the Spur and crossing over the saddle to Husband Hill, while characterizing rocks and outcrops in detail to understand their origins and the role of water in formation and modification (Figure 3).

[13] Spirit reached the base of the West Spur during the Martian southern hemisphere fall season, when the sun was north relative to the landing site latitude (subsolar latitude on Mars is 24.5 degrees north at the southern winter solstice; Figure 5). Because of the relatively poor solar situation and steady accumulation of dust on the solar panels [*Arvidson et al.*, 2004a], the time for operations was necessarily restricted relative to earlier phases of the mission. Further, the rover was typically commanded to stay on slopes with north-facing surface normals (informally called "lily pads") to maximize receipt of sunlight on the solar panels. This situation dictated a path onto the West Spur, Husband Hill, and the saddle between the Spur and Husband Hill that kept the vehicle on northern and northwest slopes (Figure 3). This constraint was alleviated in the late winter, between sol 419 and 420, when wind gusts removed much of the dust on the solar panels and increased power availability by approximately a factor of two (Figure 5) [*Greeley et al.*, 2006]. Additionally, the migration of the sun southward as the rover conducted operations through the winter and into the spring season further alleviated the need to stay on slopes with north-facing components. Interestingly, the wind event that eroded dust from the solar panels happened during the same time interval when imaging observations showed the development and movement of dust devils in the vicinity of the rover (Figure 6).

[14] Initial observations at the base of the west flank of the Spur included the rocks Pot of Gold and the nearby Breadbox located on the rim of Hank's Hollow. These measurements were followed by a brief traverse to the north to the group of rocks that included Wooly Patch, where additional measurements were conducted. Rocks exposed higher up on the northwest flank of the spur were then accessed, including an extensive measurement campaign on an outcrop in the Clovis area, followed by continued ascent of the Spur and measurements on the rocks Ebenezer, Tetl, Uchben, and Lutefisk (Figures 4 to 5 and Table 3). On sol 311 the rover descended the eastern flank of the Spur and drove onto the saddle between the Spur and Husband Hill. Spirit then traversed to the northwest flank of Husband Hill and measurement campaigns were conducted on the rocks Wishstone, Champagne, Peace, and Alligator. Paso Robles bright soil deposits were first examined on sol 400. The rover returned for further measurements on sol 424 after initial measurements of areas disturbed by the rover wheels during traverses suggested that the materials exhibited very unusual elemental and mineralogical properties.

[15] Perhaps the most important set of rock outcrops encountered by Spirit consist of Larry's Lookout, Methuselah, and Jibsheet, located approximately 50 m above the plains (Figure 4). These deposits dip conformally with topography, although at a slightly steeper angle than the topographic slope, and show a wide range of textural characteristics. This led to extensive rock measurement campaigns on Methuselah, Jibsheet, and Larry's Lookout outcrops (Table 2). The rock target Watchtower on the northwest flank of Larry's Lookout represented the last grinding experiment using the RAT, because telemetry returned on sol 416 showed that the grinding surfaces were worn down and thus the RAT was no longer able to grind into rocks. Subsequent RAT operations have been restricted to brushing activities.

4. Characteristics, Origin, and Evolution of the Plains

[16] As seen from orbit the landing site is located on plains on the floor of Gusev Crater (Figure 1). Crater size frequency distributions inferred from orbital data imply that the deposits formed during the Hesperian Period, ~3.5 Gyr before present [*Golombek et al.*, 2006]. Circular hollows ranging from ~1 to several meters across are found throughout the landing site and vicinity and are interpreted
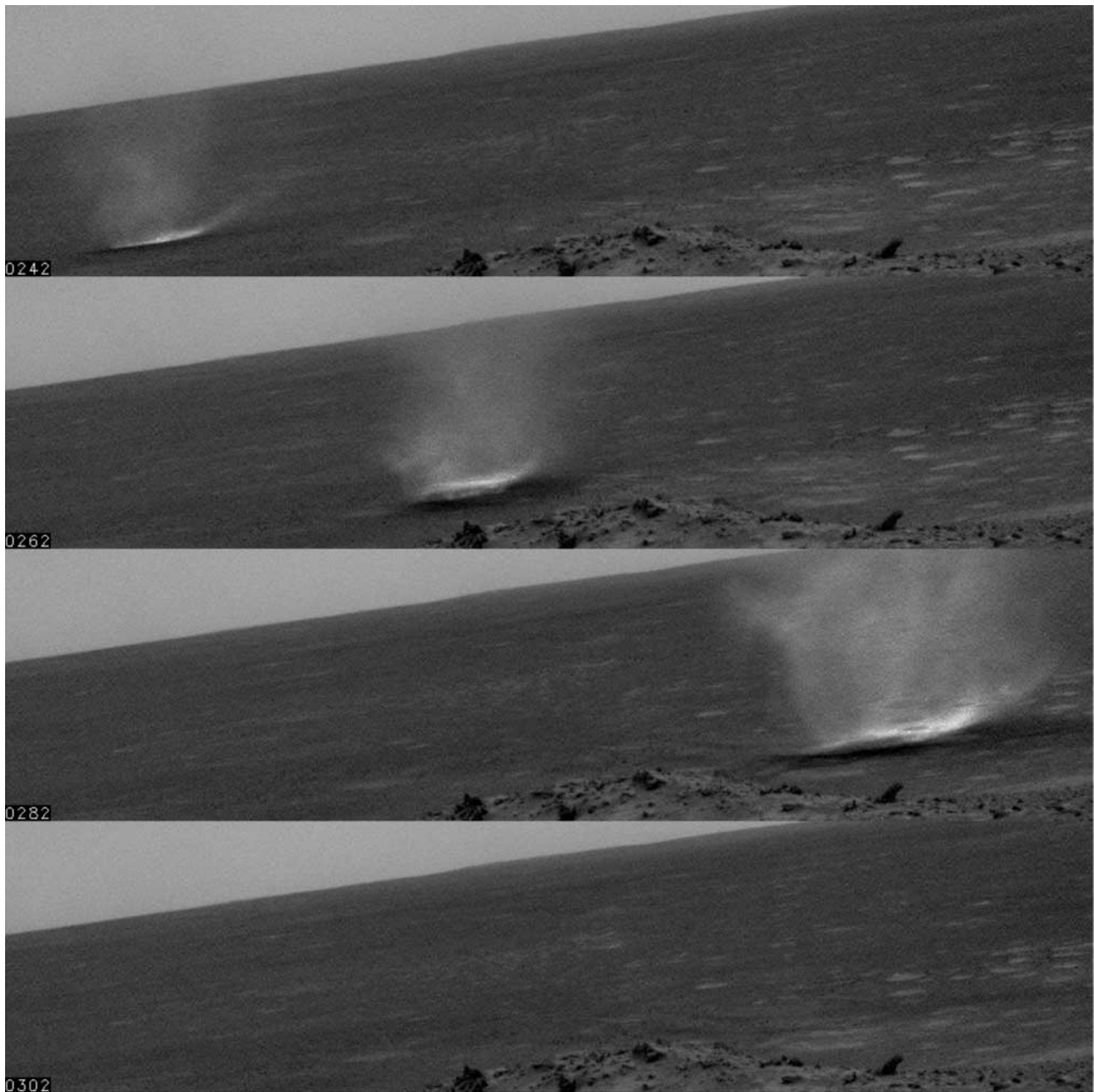
Figure 6. Dust devil sequence acquired on sol 456 at approximately noon local true solar time. The range to the dust devil was initially ∼382 m, and the probable width of the cloud was ∼70–75 m. Twenty seconds transpired between acquisition of each of these Navcam images. Frames: 2N166841489RA-DA9DWP1560L0M1, 2N166841509RADA9DWP1560L0M1, 2N166841529RADA9DWP1560L0M1, and 2N166841549RADA9DWP1560L0M1.

to be secondary and perhaps tertiary impact craters variably filled in with soil deposits [*Grant et al.*, 2004; *Golombek et al.*, 2006] (Figure 7). Rocks up to ∼1 m across are strewn throughout the immediate vicinity (∼50 m radius) of the landing site, with an areal abundance of approximately 5 percent for sizes greater than ∼1 cm, and an exponential size frequency distribution [*Golombek et al.*, 2005, 2006] (Figure 8). Rock sizes and abundances increase from the landing site to the rim of Bonneville Crater (Figure 9). Far from hollows and ejecta from larger craters, such as Bonneville, the surface is covered with evenly spaced

clasts up to a few centimeters across (Figure 8) and, at least for the several areas measured in detail using Spirit's MI, a layer of coarse-grained sand [*Ward et al.*, 2005].

[17] Rocks on the plains examined by Spirit are sitting on and partially within dust-covered soil deposits. When disturbed by the wheels the soil frequently behaves like a sheet of indurated fine-grained material a few mm thick that is being fractured and sheared by the rover [*Arvidson et al.*, 2004a]. The wheel disturbances also disrupt the dust cover and expose darker underlying materials (Figure 8). The soil beneath the dust cover consists of relatively dark, sand-
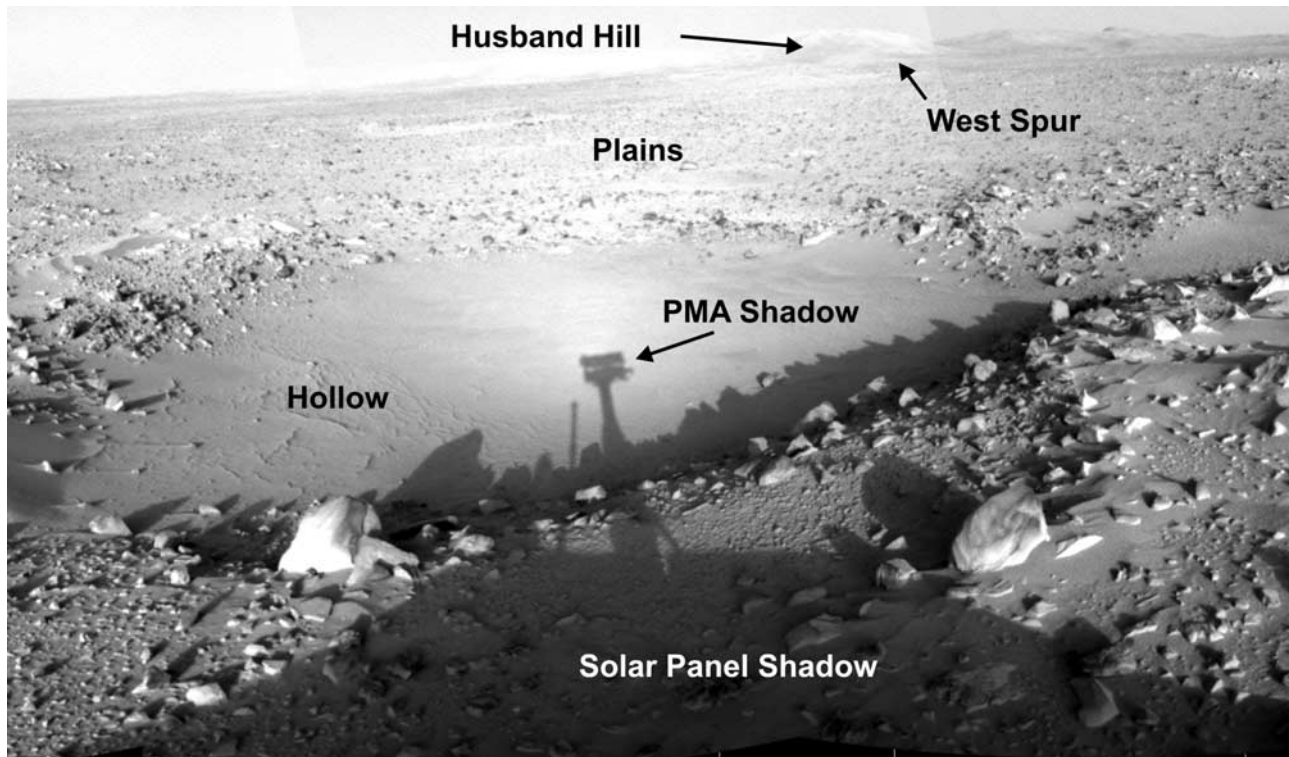
Figure 7. Backlit, afternoon Navcam mosaic looking to the east at ~10 m wide hollow on the southeastern distal edge of the Bonneville ejecta deposit. The Columbia Hills are evident to the east. Husband Hill and West Spur are labeled. Note the shadows of the Pancam Mast Assembly (PMA) and the rover's solar panels. Navcam mosaic acquired on sol 111 of frames 2N136234863FFL3600P1818L0M1, 2N136234938FFL3600P1828L0M1, and 2N136235088FFL3600P1828L0M1.
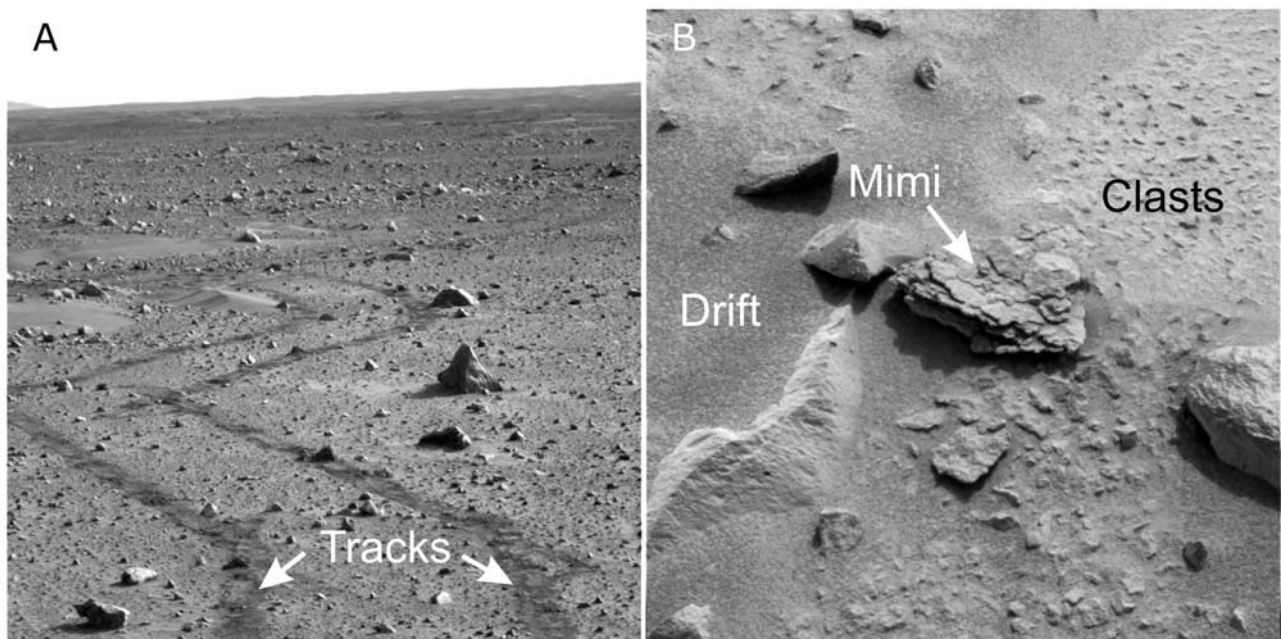

Figure 8. (a) Pancam image acquired on sol 43, looking back to Stone Council and the rock target, Mimi. Frame 2P130197480EFF0700P2402L7M1 (440 nm wavelength). (b) Pancam image of the rock target, Mimi, and surroundings, taken on sol 40. Mimi is ~12 cm wide. Note equally spaced clasts surrounding and above Mimi, along with sand-sized particles exposed on drift to left of Mimi. Frame 2P129908422EFF0500P2598L2M1 (753 nm wavelength).
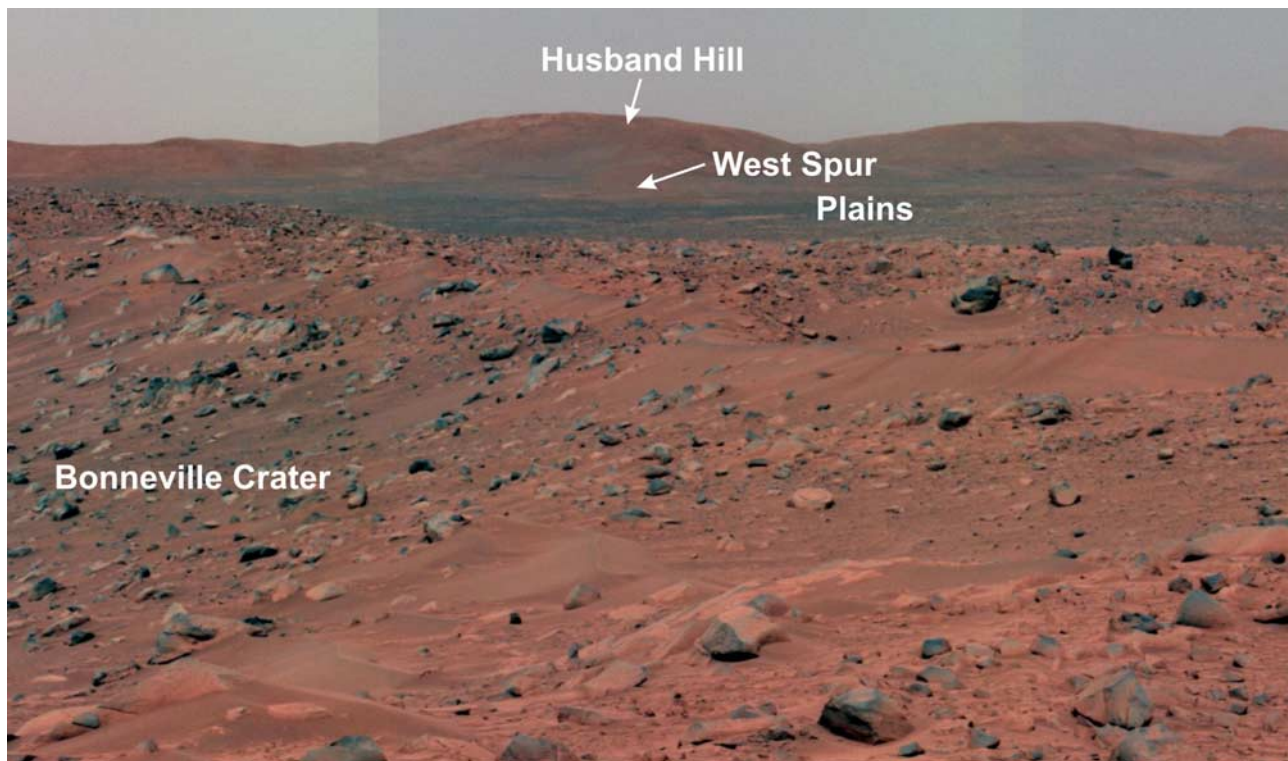
Figure 9. Portion of Bonneville crater color panorama with Husband Hill and West Spur in background to the east. False color infrared with 440 nm image as blue, 535 nm as green, and 753 nm as red.

sized material with a finer-grained component that gives the material the ability to be molded into well-defined casts by the wheel cleats and by the placement of the MB contact plate, which exerts a force of ~1 N [*Arvidson et al.*, 2004a] (Figure 10). In some cases the casts show very fine detail, including the shape of the screw head-on the MB faceplate [*Herkenhoff et al.*, 2004, 2006]. The subsurface soils also show modest degrees of cohesion, with values of ~1 kilopascal, perhaps resulting from electrostatic forces or a modest degree of cementation [*Arvidson et al.*, 2004a].

[18] Detailed measurement campaigns were conducted on four plains rocks, including Adirondack, Humphrey, Mazatzal, and Route 66 (Figure 5 and Tables 2 and 3). For the first three rocks MI, APXS, and MB data were acquired on undisturbed rock surfaces, after using the RAT to brush away loose material, and after grinding by the RAT (Figure 11). These systematic observations allowed characterization of the dust cover evident on the rocks, examination of more indurated coatings, and measurement of newly exposed rock surfaces located several millimeters below the natural surfaces. Spirit's remote sensing and IDD-based observations clearly show that the relatively fresh surfaces exposed by grinding are composed of olivine-bearing basalts [*Bell et al.*, 2004; *Gellert et al.*, 2004, 2006; *Morris et al.*, 2004, 2006; *McSween et al.*, 2004, 2006], although bright vein and vug-filling deposits were also observed even after deepest grinds (~8 mm on Mazatzal, Table 3). The olivine-bearing basalt interpretation is strongly bolstered by Pancam and MiniTES spectral observations that suggest the rocks observed by these systems on the plains are basalts with varying degrees of dust cover [*Bell et al.*, 2004; *Christensen et al.*, 2004].

[19] APXS and MB reduced data sets are inherently multidimensional in their nature and thus amenable to application of techniques that reduce dimensionality to explore key relationships. In this paper correspondence analysis techniques [e.g., *Larsen et al.*, 2000] are used to illustrate the patterns evident in the reduced data and to provide a lead-in for the detailed papers that describe and analyze the elemental abundance and iron-phase mineralogy data for rocks and soils [e.g., *Gellert et al.*, 2006; *McSween et al.*, 2006; *Ming et al.*, 2006; *Morris et al.*, 2006; Klingelhöfer et al., manuscript in preparation, 2006]. Correspondence analysis is a normalized factor analysis procedure in which factor loadings for both variables and samples can be presented on the same scatterplots (Figures 12a–12c). For this paper the analysis was run for oxide abundances for all APXS and MB rock and soil measurements, except for the Paso Robles soil deposit. Paso Robles is so unusual that it will be described separately in this paper. Analyses through sol 512 were included in the correspondence analysis runs. Factor loadings for variables and samples for factors one and two were found to explain ~70% of the variance for both data sets and thus illustrate first-order trends among variables and samples (Figures 12a–12c).

[20] APXS results for plains rocks and soils, expressed as oxides, exhibit a trend in which abraded ("ratted") surfaces of Adirondack, Humphrey, and Mazatzal rocks plot as end-members and in a quadrant of the scatterplot where elements associated with basaltic compositions are expected (Figure 12a). The chromium content of these surfaces is
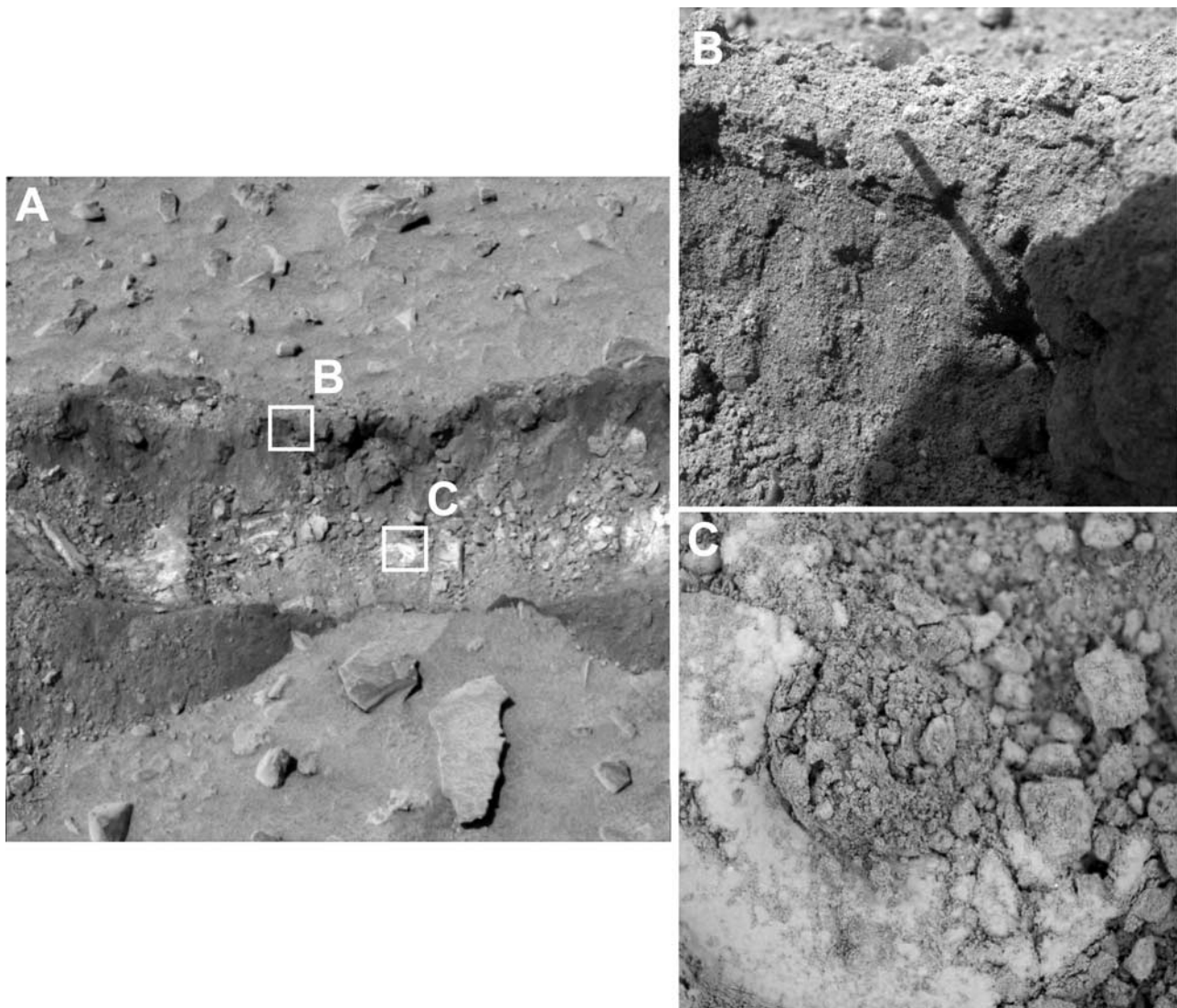
Figure 10. (a) Pancam image of the middle portion of the Big Hole trench mosaic with boxes showing location of Microscopic Imager frames shown in Figure 10b for the trench wall and Figure 10c for the floor. Mössbauer Spectrometer contact plate imprint is evident on the trench floor. Note the equally spaced rock clasts on the surface above the trench wall. Frame 2P136663464EFF37CCP2404L2C1 (753 nm wavelength). (b) Microscopic Imager view of the undisturbed surface and trench wall of the Big Hole trench. The surface is covered with relatively coarse grains as compared to the trench wall. Frame 2M136662584EFF37CAP2957M2M1. (c) Microscopic Imager view of the Big Hole trench floor, centered on the Mössbauer Spectrometer imprint of the contact plate. Note how the plate molded the soil, consistent with the presence of sand-sized grains with finer grained filling the pores. Frame 2M136501952EFF37CAP2957M2M1.

clearly a distinctive aspect of these relatively fresh surfaces. The MB-based iron mineral abundances for the abraded surfaces of the three rocks also plot as sample end-members, with olivine and, to a lesser extent, pyroxene and magnetite as distinctive minerals (Figures 12b and 12c). Adirondack Class is the name given to these plains basalt rocks [*Squyres et al.*, 2006].

[21] MI, APXS, and MB measurements were conducted on Adirondack, Humphrey, and Mazatzal (1) before RAT operations to determine the characteristics of undisturbed surfaces, (2) after brushing to remove relatively loose material, and (3) after abrasion with the RAT to expose

relatively fresh surfaces. The patterns observed in APXS and MB data are also useful for understanding the nature of dust and indurated coatings on rocks. Consider that in the APXS-based correspondence analysis scatterplot the undisturbed surfaces "Oregon" and "New York" on the rock Mazatzal have the largest displacement from the deepest abrasion surface and plot in the soil portion of the diagram. Further, the brushed surface for Mazatzal plots close to the undisturbed surfaces, whereas the location of the first abrasion (Maz-Abrade-1; relatively shallow as compared to Maz-Abrade-2; see Table 3) plots between the brushed surfaces and the more deeply abraded surface.
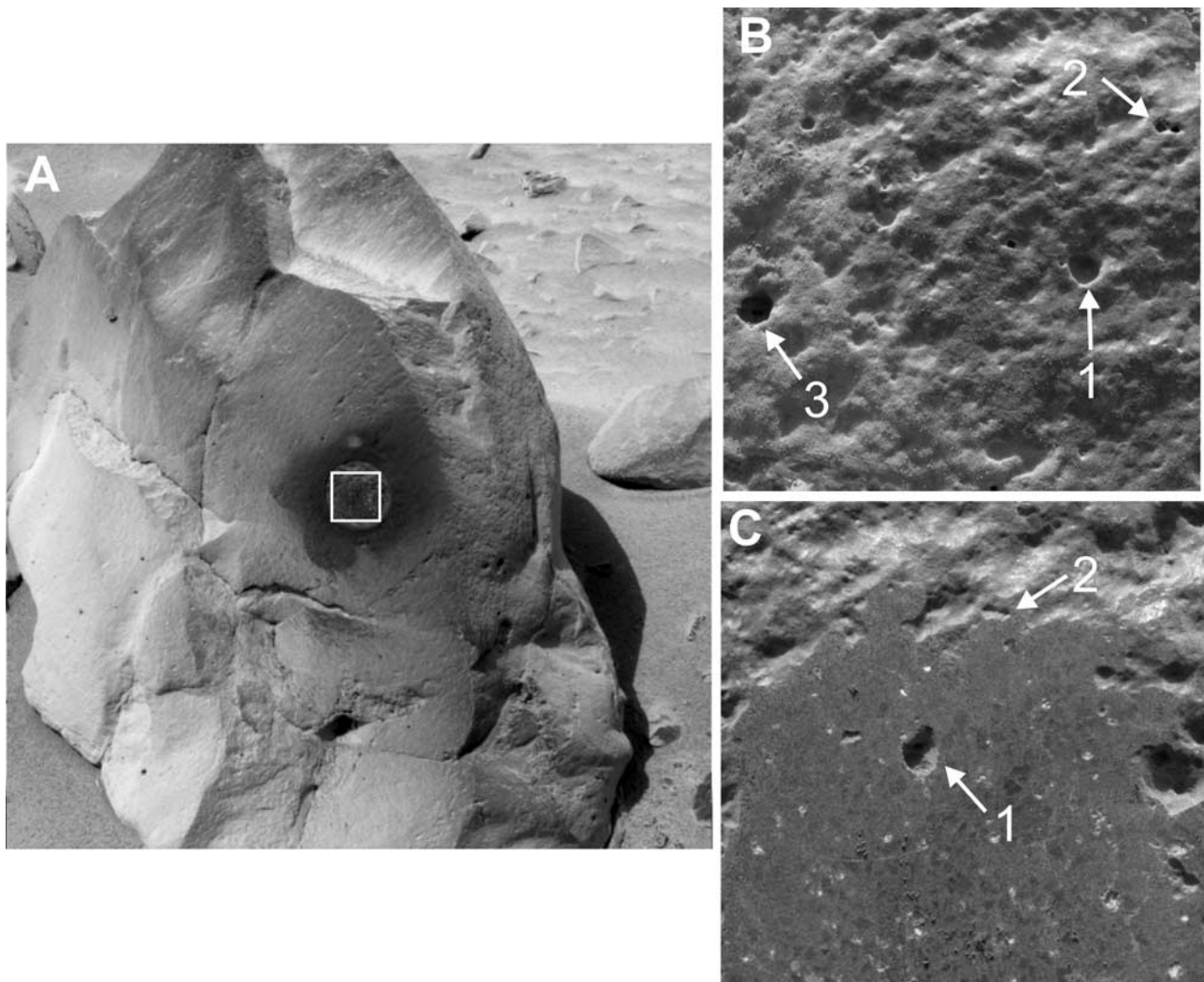
Figure 11. (a) Pancam image of the rock Humphrey taken on sol 60 after RAT grinding operations were completed. Note the dark nature of the RAT "droppings" and hole relative to the surrounding rock. Humphrey is ~70 cm high. RAT hole is 4.5 cm across. White box shows region covered by MI's in Figures 11b and 11c. Pancam frame 2P131696667EFF1159P2597L2M1 (753 nm wavelength). (b) Microscopic Imager view acquired on sol 57 of the brushed surface of Humphrey. Locations 1 and 2 show voids also shown in Figure 11c. Location 3 shows void with hexagonal shape consistent with former presence of olivine phenocryst. Frame 2M131421248EFF1155P2939M2M1. (c) Microscopic Imager view acquired on sol 60 of the abraded surface of Humphrey after grind. Frame 2M131690397EFF1155P2939M2M1.

For the MB-based scatterplot the trend from abraded to undisturbed surfaces is away from olivine and toward nanophase iron oxide (Figure 12c). Humphrey abraded, brushed, and undisturbed surfaces (Figures 11 and 12a–12c) show similar trends as found for Mazatzal, but over a much more limited range relative to the fresh end-member. The patterns are consistent with the textural evidence observed in MI data, which show a relatively loose, thin dust coating on Humphrey and the presence of an indurated, relatively thick (~1 mm) dark coating beneath the loose dust cover on Mazatzal [*Arvidson et al.*, 2004a; *McSween et al.*, 2004].

[22] Plains soil analyses cover a range of locations on the APXS scatterplot, with a swarm that extends from the fresh rock end-member to locations where sulfur and chlorine become distinctive compositional parameters (Figure 12a). The high sulfur and magnesium enriched end-member is represented by the floor and wall of The Boroughs Trench. Plains soils on the MB-based scatterplots cluster tightly along the olivine vector, with The Boroughs analyses displaced toward nanophase iron oxides (Figures 12b and 12c).

[23] Results from the rock and soil campaigns, including the textural evidence and the elemental and mineralogical trends discussed above, suggest that soluble species have been mobilized and deposited onto rock surfaces and have concentrated in some subsurface soils. The relative softness of the rocks as compared to hard terrestrial basalts also supports the idea that the surfaces have been altered [*Arvidson et al.*, 2004a]. The processes affecting the surfa-
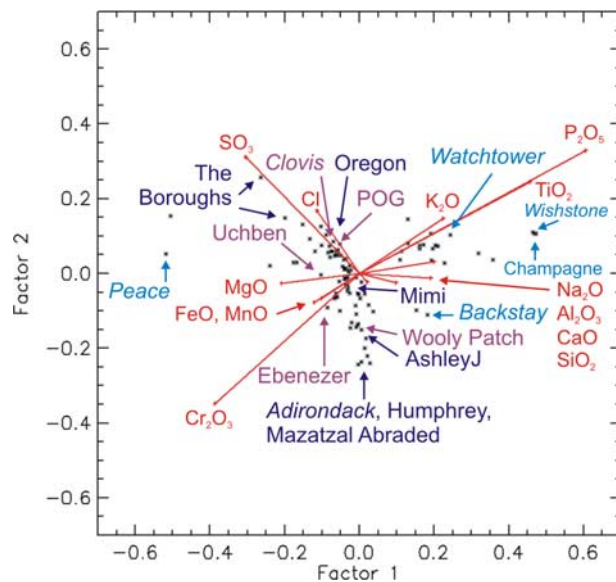
Figure 12a. First two factors and associated locations of variables (solid lines) and samples (stars) as generated by a correspondence analysis applied to oxide compositions from APXS rock and soil observations [*Gellert et al.*, 2006]. Rock names are located next to analyses conducted on abraded or brushed (Methuselah-Keystone) surfaces for all but Mimi (undisturbed surface), Oregon (one of the undisturbed surfaces on Mazatzal), and AshleyJ (undisturbed surface on Humphrey). Br, Ni, Zn, and Br were not included in the analyses to simplify patterns. Words in italics designate samples that define rock classes. Blue letters are for data from the plains, purple from West Spur, and cyan from Husband Hill.
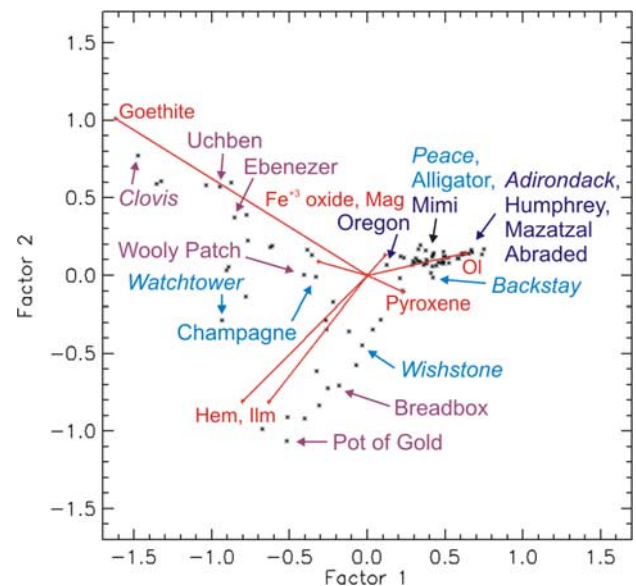

Figure 12b. First two factors and associated locations of variable (solid lines) and samples (stars) as generated by a correspondence analysis applied to iron-phase mineralogy inferred from MB rock and soil observations [*Morris et al.*, 2006]. Rock names are located next to analyses conducted on abraded surfaces for all but Mimi, Breadbox, and Oregon, which are undisturbed surfaces, and Backstay, which was brushed before measurements were acquired. Note the importance of olivine, hematite, and goethite in variable space and the extent to which rock samples follow these patterns.

ces and outer portions of the rocks most likely involved relatively low water to rock ratios and may have occurred via thin films of water [*Hurowitz et al.*, 2006]. Possibilities include volatile migration when the surfaces were covered by dirty snow, as is expected during periods of high obliquity, and processes related to migration of soluble species in frost-vapor transfer onto and from rock surfaces [*Arvidson et al.*, 2004a; *Haskin et al.*, 2005; *Yen et al.*, 2005].

5. Characteristics, Origin, and Evolution of the Columbia Hills

[24] The Columbia Hills reach up to ~120 m in elevation above the plains landing site and ~90 m above the plains just to the west of the West Spur (Figures 1–3). Orbital observations show that the Hills rocks are clearly embayed by the olivine-bearing basaltic plains materials and thus represent the oldest geologic unit encountered by Spirit during its mission (Figures 1–3). The first geomorphic unit encountered in the Columbia Hills was the West Spur (Figures 2 and 3) and the initial rocks examined were on the rim of Hank's Hollow at the base of the Spur, including the rocks Pot of Gold and Breadbox (Figure 13). These rocks are very different in appearance from the plains rocks. In particular, Pot of Gold and Breadbox are texturally
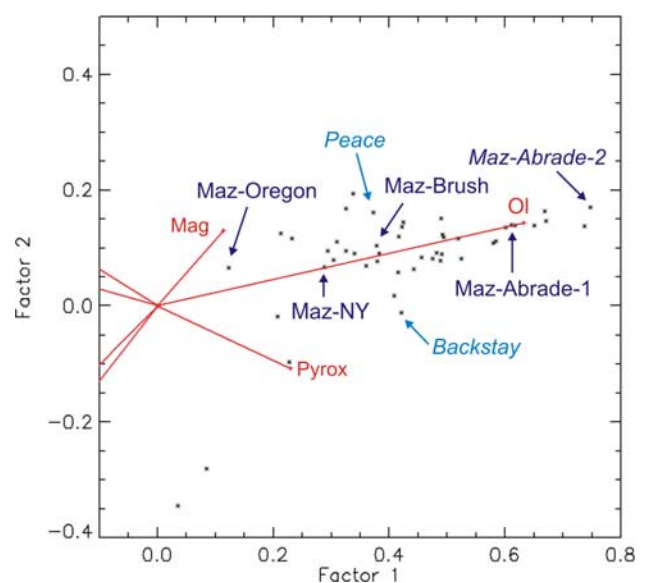

Figure 12c. Blow-up of olivine-dominated area shown in Figure 12b, with locations of data for the deepest abrasion of Mazatzal (Abrade-2), the first abrasion (Abrade 1), the postbrush measurement (Brush), and data for two undisturbed areas (NY and Oregon).
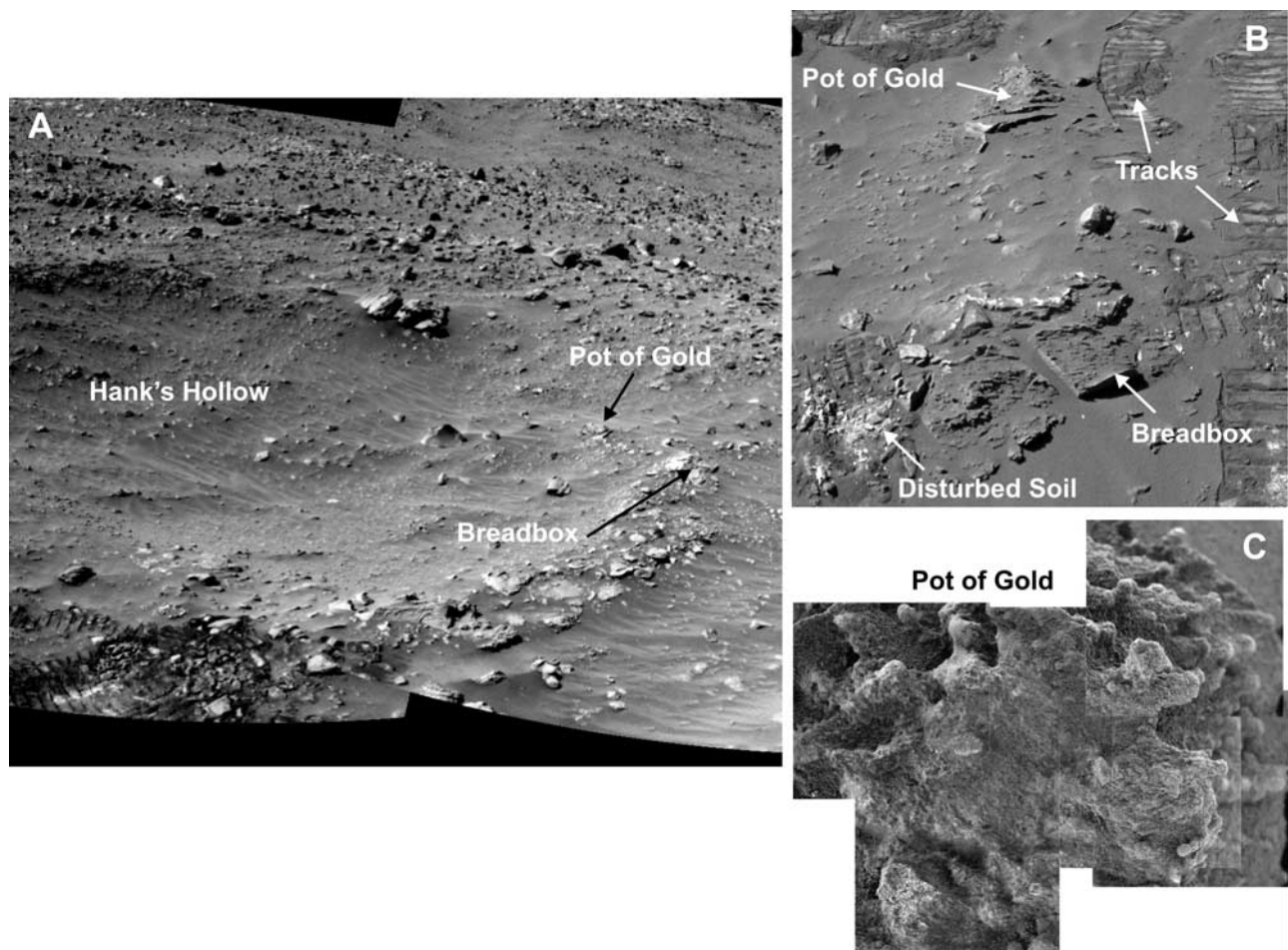
Figure 13. (a) Navcam image mosaic of Hank's Hollow at the base of the West Spur, Columbia Hills. Pot of Gold and Breadbox are two rocks on the rim of the Hollow that were the target of IDD measurements. Frames 2N140212820EFF6800P0665L0M1 and 2N140212918EFF6800P0665L0M1. (b) Pancam image of Pot of Gold and Breadbox. Also shown are soil deposits disturbed by rover tracks. Frame: 2P141099804EFF6962P2530L7C1 (440 nm wavelength). (c) Postgrind Microscopic Imager image mosaic of Pot of Gold, acquired on sol 171, after several of the knobs or stalks were broken by an attempted grind by the RAT. Mosaic covers ~7 cm in width.

complex, have a granular appearance, and Breadbox has sides that are topographically higher than its interior. Grinding Pot of Gold produced minimal results because of the soft nature of the material and the irregular (stalk-like) nature of the surface encountered. Pot of Gold, Breadbox and the surrounding rocks appear to have been subjected to a type of cavernous weathering in which the relatively soft interiors have been significantly eroded by wind, whereas the more resistant exteriors still remain. One way to generate this differential resistance is to preferentially case-harden (cement) the exteriors of the rocks and/or corrode the interiors. Fluid-related phenomena would enhance either of these processes. Pot of Gold and Breadbox are also mineralogically distinct from the plains rocks (Figures 12a–12c and Table 3). In particular, Pot of Gold and Breadbox are relatively weak rocks that are highly enriched in hematite and nanophase iron oxides, and depleted in olivine relative to plains rocks [*Morris et al.*, 2006; Schröder et al., manuscript in preparation, 2006; Ruff et al., manuscript in preparation, 2006].

[25] Wooly Patch was the next focus for rock measurements and was found in outcrop to the north and slightly uphill from Hank's Hollow (Tables 2 and 3). Wooly Patch is a granular, fine-grained and relatively soft rock characterized by the presence of nanophase iron oxides, hematite, and goethite, in addition to pyroxene and magnetite [*Morris et al.*, 2006]. Olivine is only a minor component (Ruff et al., manuscript in preparation, 2006). Further, analyses of APXS data suggest that phyllosilicate phases could be present [*Wang et al.*, 2006b]. Interestingly, Pot of Gold, Breadbox, and Wooly Patch fall along an elemental abundance mixing line between the plains rocks and The Boroughs trench data (Figure 12a). This suggests that the rocks at the base of the West Spur have compositions matched by combining olivine-bearing basalt and alteration phases, but they have rather different emplacement and/or modification histories than plains materials, given the distinctive mineralogy (Schröder et al., manuscript in preparation, 2006).

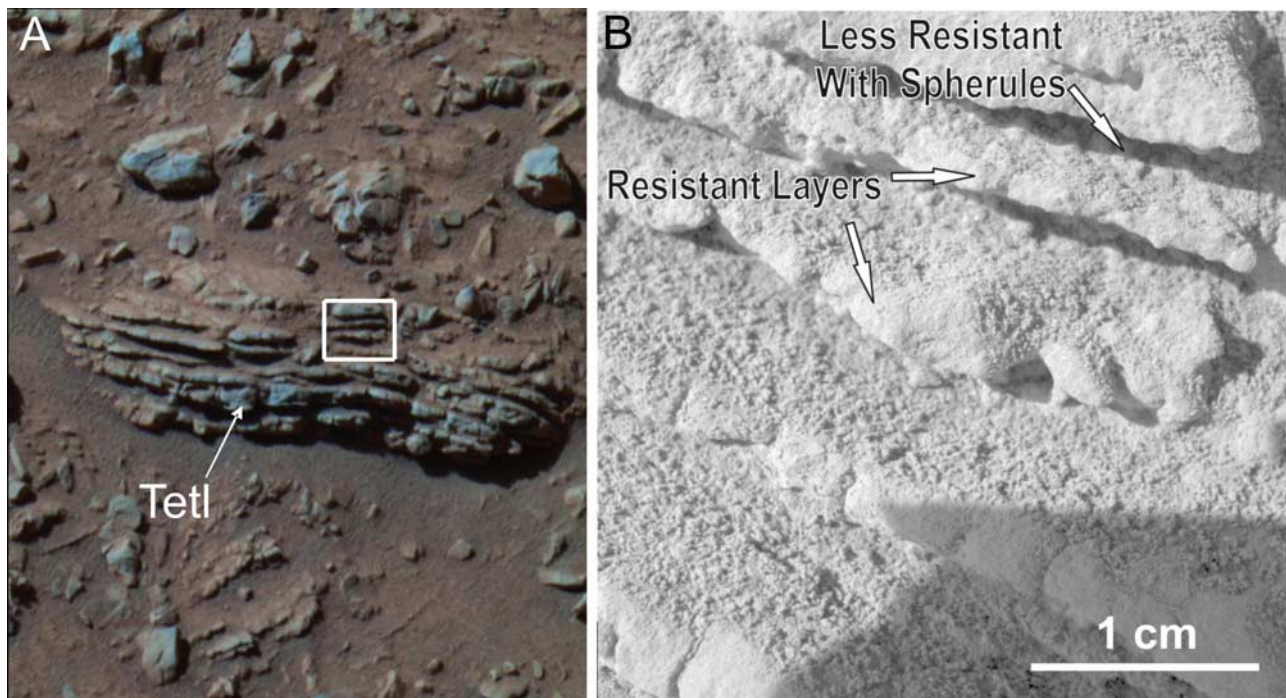[26] The next major rock experiment conducted was in the Clovis area on the upper west slope of the West Spur

Figure 14. (a) False color infrared Pancam image composite of Tetl. The rock is about 10 cm high. Frames 2P149802707ESF45P2598L2C1 (753 nm), 2P149802707ESF45P2598L5C1 (535 nm), and 2P149802707ESF45P2598L7C1 (440 nm) assigned to red, green, and blue colors in the composite. (b) Microscopic Imager mosaic of a portion of Tetl. Note discrete layers and possible large grains at base of more massive and presumably more resistant layers. Frame: 2M150519068EFF8953P2906M2M1.

(Figure 3 and Table 3). The Clovis rock target is platy and conformable to topography, either due to layering or exfoliation. Clovis is the "type" rock for the Clovis Class of rock materials [*Squyres et al.*, 2006]. What distinguishes Clovis from other rocks is the abundance of goethite (Figure 12). Other rocks examined in the target-rich environment that Spirit encountered as it ascended the Spur included Ebenezer, Tetl, Uchben, and Lutefisk (Figures 14 and 15), all of which show enrichments in goethite relative to the ensemble of rocks examined during Spirit's mission (Figure 12b). Uchben was part of a densely jointed or layered suite of rocks. All of the rocks examined on the Spur are granular, poorly sorted, matrix-dominated (based on MI's of abraded surfaces of Clovis and Uchben), and contain rounded to irregularly shaped grains (Figure 15). This suite of rocks are also related in terms of enrichment in goethite relative to plains rocks and rocks topographically beneath the Clovis outcrops (Figure 12b), particularly relative to Pot of Gold. Spur rocks are also enriched in nickel as compared to plains rocks [*Ming et al.*, 2006]. Descent from the Spur on its eastern side showed outcrops that have exfoliation patterns or layers that also dip conformably with topography, i.e., toward the east.

[27] Ascent onto the northwest flank of Husband Hill to the Cumberland Ridge was accompanied by a suite of additional rock measurements, including the rocks Wishstone and Champagne, which were found to be soft, granular rocks characterized by relative enrichment in phosphorus and titanium and the presence of pyroxene, olivine, hematite, nanophase iron oxides, magnetite, and ilmenite (Figures 12a–12c and Table 3). The Wishstone Class is meant to characterize this type of material [*Squyres et al.*, 2006]. Peace and Alligator are rocks that have iron-bearing phases consistent with the plains basalts, although Peace (which denotes the Peace Class [*Squyres et al.*, 2006]) is enriched in bromine, chlorine, sulfur, and magnetite relative to plains rocks (Figures 12a–12c). In addition, MiniTES data for Peace show evidence for bound water based on an absorption feature at 1650 cm^{-1}. A very important discovery as the rover continued its ascent of Husband Hill along the NW-SW trending Cumberland Ridge was the set of Methuselah, Jibsheet, and Larry's Lookout outcrops (Figure 16). These deposits have bedding planes that dip in the direction of the topographic slope, although at larger angles than the slope. Watchtower, a rock target on Larry's Lookout, is enriched in phosphorus and titanium-bearing phases such as ilmenite, together with nanophase iron oxides and hematite (Figures 12a–12c) and denotes the Watchtower Class [*Squyres et al.*, 2006]. Other rocks in these outcrops were also found to be enriched in phosphorus and titanium, together with hematite and ilmenite. The final target examined along the Cumberland Ridge is the float rock, Backstay. Backstay is a new class of basaltic materials that is enriched in SiO_2 and Al_2O_3 relative to Adirondack Class rocks.

[28] The observations thus far indicate that rock surfaces on both the West Spur and Husband Hill are largely conformable with topography. The outcrops exposed along the Cumberland Ridge provide the best evidence that actual outcrop as opposed to float rocks are exposed. The layering, presence of granular textures, abundance of hematite and
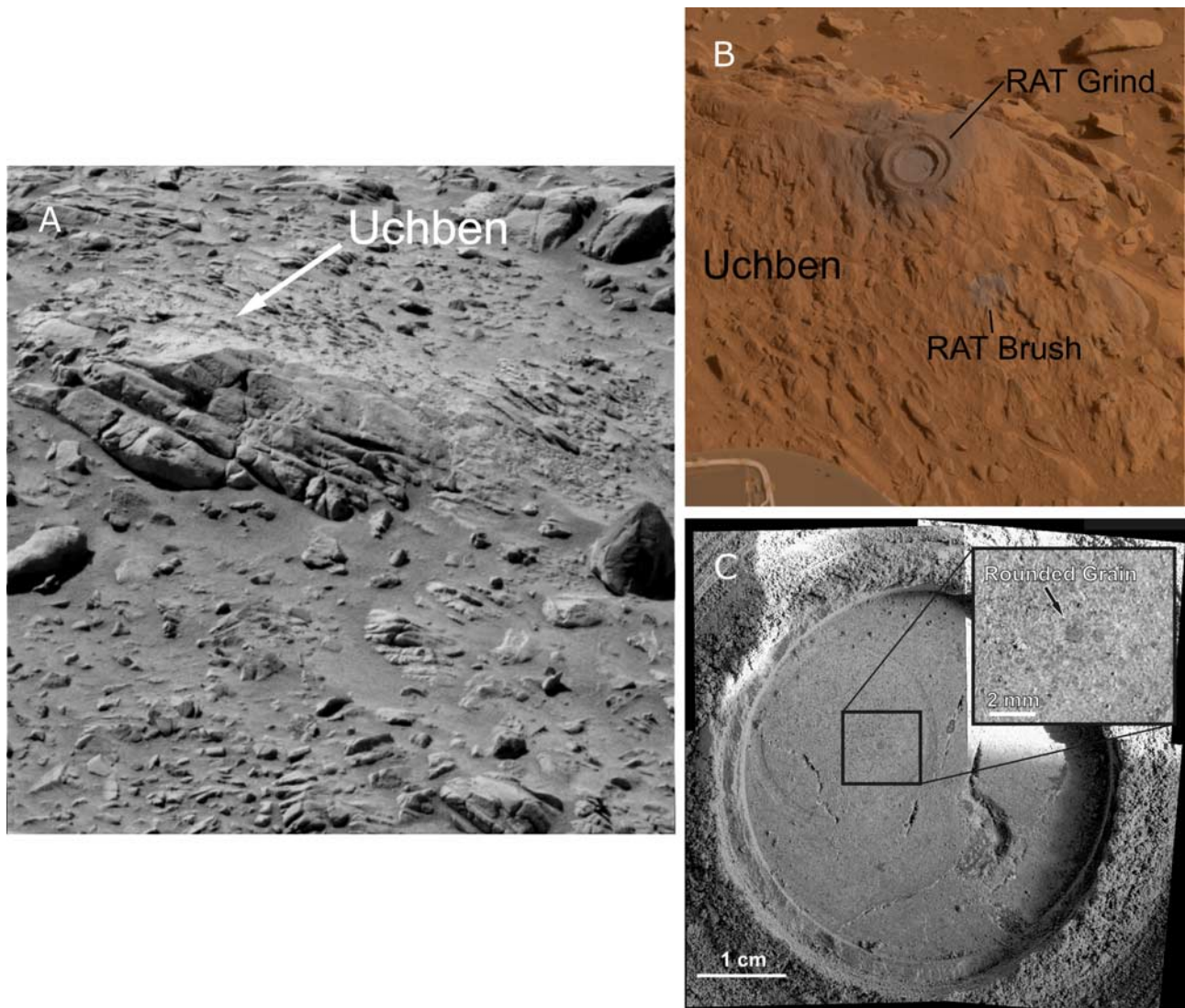
Figure 15. (a) Pancam image of Uchben. Frame 2P151044793EFF8982P2415L2C1 (753 nm wavelength). (b) Pancam-based false color infrared composite of Uchben after RAT brush and grind activities. Frames 2P152381928EFF8992P2543L2C1 (753 nm), 2P152381928EFF8992P2543L5C1 (535 nm), 2P152381928EFF8992P2543L7C1 (440 nm) assigned to red, blue, green, and blue colors. (c) Microscopic Imager mosaic of the abraded Koolik surface on Uchben, acquired on sol 286. Note the granular textures. Frames 2M151760506EFFP2957M2M1, 2M151759602EFF8987P2936M2M1, 2M151759825EFF8987P2957M2M1, and 2M151760354EFF8987P2936M2M1.

goethite, coupled with enhanced values of soluble species (Br, Cl, S, P) suggest that the rocks composing the Columbia Hills are crustal sections that formed by volcaniclastic processes and/or impact ejecta emplacement. These rocks have also been modified in an aqueous environment, most likely in an acid-sulfate dominated environment [*Ming et al.*, 2006; *Morris et al.*, 2006; *Hurowitz et al.*, 2006]. This conclusion is consistent with Pancam-based analyses that suggest at least some of the rocks have spectral properties comparable to terrestrial basaltic volcanic tuff deposits [*Farrand et al.*, 2006]. The enhanced nickel content in West Spur rocks adds support for an impact origin or access to source rocks with an ejecta component [*Ming et al.*, 2006]. We note that wind and perhaps water transport may have also been involved in emplacement of rocks encoun-tered thus far, although unique evidence for these processes has thus far been elusive.

[29]   Measurements of surface soils while Spirit was in the Columbia Hills show that these deposits are indistinguish-able from plains soils, i.e., dominated by olivine-bearing basalts with varying amounts of alteration phases (Figures 12a–12c). Wind and perhaps impact processes have ho-mogenized the soils over at least the ~4 km length scale traversed by Spirit and perhaps over even longer length scales [*Yen et al.*, 2005]. Transport of soil into the Hills must have happened at a faster rate than break-down of local rocks since the measurements show little addition of local materials. There is one exception and that is associated with measurements in the Paso Robles soil scuffed and exposed by the rover wheel (Figure 17). The Paso Robles soil
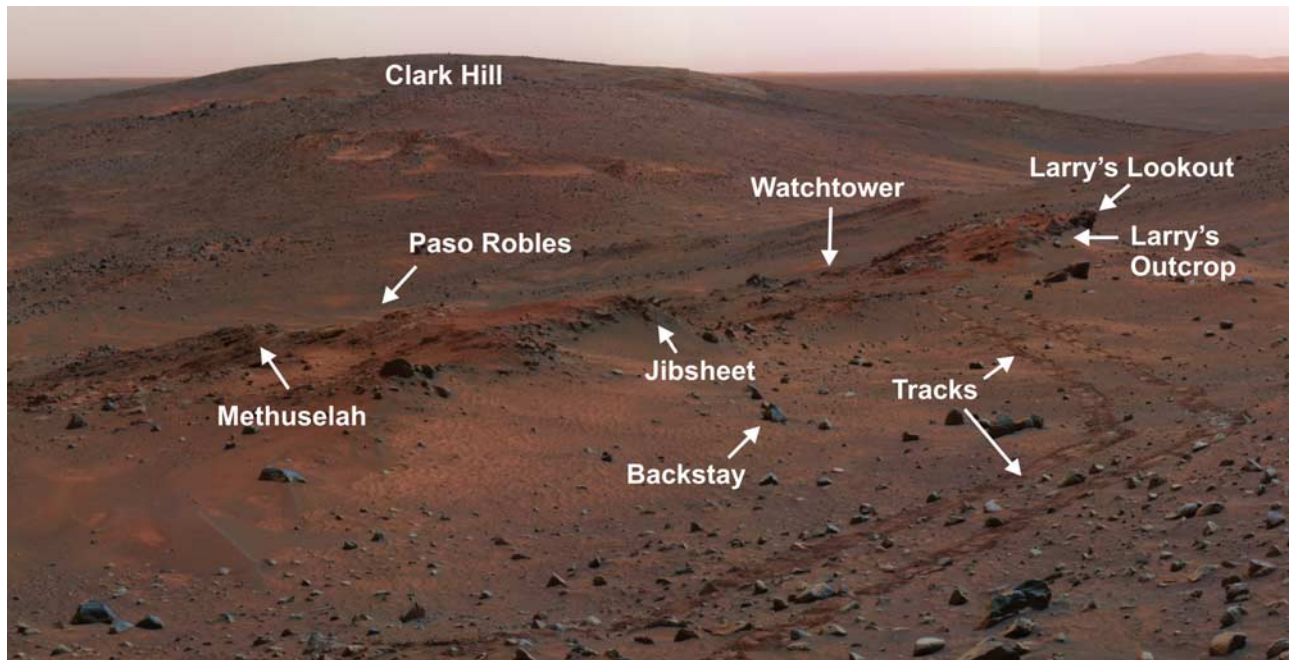
Figure 16. Pancam mosaic acquired on sol 454 of the Methuselah, Jibsheet, and Larry's Lookout outcrops showing layers dipping in the same direction as the topography. Also shown are the locations for acquisition of in situ observations for Paso Robles (downhill of the outcrops) soil, Watchtower, and Backstay. False color infrared with 440 nm image as blue, 535 nm as green, and 753 nm as red.

deposits are dominated by iron sulfates of hydrothermal or aqueous origin that were either produced locally or produced elsewhere and transported in to the current site (e.g., via wind or impact) [*Ming et al.*, 2006; *Morris et al.*, 2006]. MiniTES data reinforce this conclusion with strong and unique (for soils) evidence for the presence of bound water based on the $1650 \ cm^{-1}$ absorption feature. Finally, it is noted that measurements on undisturbed, brushed, and abraded surfaces for rocks on the Columbia Hills did not produce the wide range of compositions and iron-phase mineralogy encountered as a function of depth for the plains rocks, indicating that the Hills rocks have close affinities to dust and coatings.

6. Magnetic Properties Experiment Results

[30] Both airborne dust and dust produced by brushing and grinding with the RAT has been investigated using the seven magnets on the rover (see Tables 1 and 2). The magnetic properties experiments have shown that few, if any, particles are not influenced by the presence of the strong magnetic field produced by the sweep magnet. This means that essentially all particles suspended in the atmosphere are somewhat magnetic [*Bertelsen et al.*, 2004]. Also, the experiments have shown that although all particles are magnetic they are not equally strongly magnetic; the filter and capture magnets are sufficiently different in their interaction with the airborne dust that they attract somewhat different populations of the airborne particles. The filter magnet is to some degree able to separate out a more strongly magnetic (and darker) fraction of the particles. These darker particles are also found near the rim of the active surface of the capture magnet, whereas the spectra of the dust on most of the surface of the capture magnet are
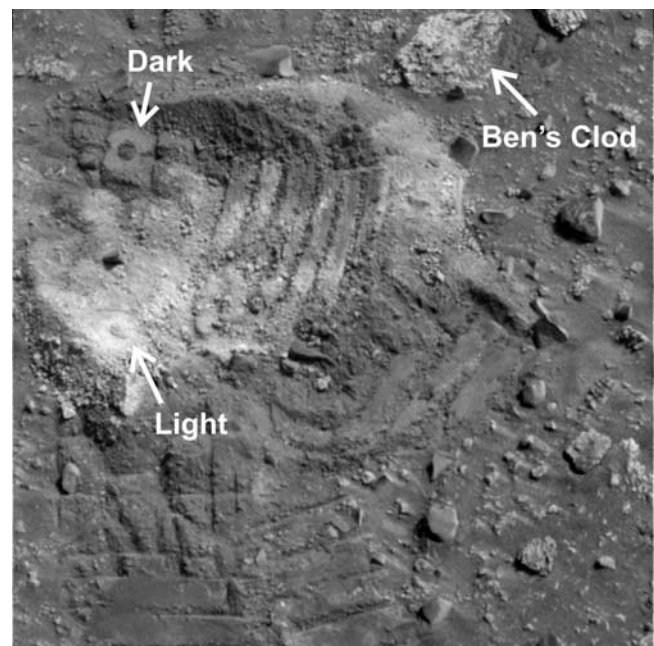

Figure 17. Pancam image of the Paso Robles area showing regions disturbed by rover wheels and exposing bright materials with strong Fe and Mg sulfate signatures. MB contact plate imprints evident on the bright materials and a more typical, darker soil. Ben's Clod is an ~10 cm wide rock that is enriched in phosphorus and titanium and coated with sulfur-bearing materials, based on APXS observations [*Gellert et al.*, 2006]. Frame 2P164633207EF-FA8B5P2530R2M1.

similar to those of the finest particles seen on the surface [*Bertelsen et al.*, 2004].

[31] Mössbauer and APXS spectra have shown that the dust captured by the magnets contain substantial amounts of nonmagnetic or very weakly magnetic minerals and that the mineral mainly responsible for the magnetic properties of the airborne dust is nonstoichiometric magnetite [*Goetz et al.*, 2005]. Among the minerals found in the dust of the magnets is olivine and the magnetite appears similar to the nonstoichiometric magnetite found in the basaltic rocks in Gusev Crater. This leads to the conclusion that the airborne dust originated in a dry environment and that water did not play any significant role in the processes that formed the dust [*Goetz et al.*, 2005].

7. Atmosphere-Surface Dynamics

[32] The area surrounding the landing site has a relatively low, but variable albedo, with numerous dark tracks extending to the southeast from craters (Figures 1 and 2). The tracks are interpreted to result from dust devils that erode the thin, bright dust deposits evident from Spirit's observations [*Greeley et al.*, 2006]. Also, as noted, dust devils have been observed directly by Spirit (Figure 6). Measurements of the lower atmosphere temperature profiles using the MiniTES instrument on Spirit showed that a superadiabatic layer forms in the bottom 100 to 200 m of the atmosphere during the period from about 9:00 until about 16:00 [*Smith et al.*, 2004]. Temperatures within this layer can fluctuate by several degrees on a time-scale of a minute or less. The superadiabatic profiles are inherently unstable and lead to convective motions within the lower atmosphere. This situation, coupled with the strong slope winds associated with the plains within Gusev Crater, are likely the reasons for the abundance of dust devil activity at and around the landing site.

[33] During the course of the Spirit mission atmospheric dust slowly accumulated on the solar panels [*Lemmon et al.*, 2004; *Arvidson et al.*, 2004a]. As noted during sols 419 and 420 some of the dust was removed by high winds, leading to a twofold increase in power. A marked decrease in surface albedo at the Paso Robles site was also observed after the wind event [*Johnson et al.*, 2006]. Further, the rover was parked from sols 395 to 397 to receive flight software uploads. Imaging with Pancam and MI of the parked area and a soil-covered region with a MB faceplate imprint before and after the upload showed some aeolian redistribution of material. This suggests that the Gusev plains are the site of an active aeolian environment. On the other hand, the presence of evenly spaced clasts on soils and coarse sand covers on aeolian bedforms suggests that wind only rarely is able to change the surface to a significant extent [*Ward et al.*, 2005]. The reason is that the large grain sizes associated with these surface layers require enormous wind shear under the very thin atmosphere. High winds that significantly change the configuration of these materials must be very rare indeed or relegated to earlier climates with high atmospheric densities.

[34] Finally, we note that the well-known aphelion cloud belt that is clearly visible from Earth and orbit [*Wolff et al.*, 1999] has been very difficult to observe from the surface. Discrete clouds were rarely observed by Spirit even when the presence of water ice was detected using MiniTES and observed concurrently from orbit. This situation may be analogous to terrestrial "subvisual cirrus" clouds, which are believed to play an important role in climate issues through their infrared radiative properties, but are equally difficult to observe.

8. Summary of Key Results

[35] The Spirit mission has unequivocally validated the importance of mobility and use of an integrated payload to conduct surface science. For example, consider that it took 157 sols of operations and ∼3 km of traverses to reach the Columbia Hills, where the strongest evidence for the interaction of rock and water was found. Without this range of mobility the primary science objective focused on understanding the role of water in modifying crustal materials would have been much more difficult to achieve. As another example, it took the combination of measurements provided by the entire Athena payload to define in detail the nature of coated and fresh surfaces for the rocks encountered by Spirit as it traversed the plains and Hills. Likewise, it has taken the ensemble of measurements from the entire payload to decipher the nature of the rocks encountered in the Hills, including the textural, mineralogical, and elemental abundance evidence that led to the conclusion that these materials have been altered in an aqueous environment.

[36] The most important scientific results to date from the Spirit mission are briefly summarized below:

[37] 1. Plains rocks are dominated by primitive olivine-bearing basalts with surfaces that are coated to varying degrees. Near-surface vugs and cracks are filled with bright materials. These surface materials were emplaced, at least in part, through the action of thin films of water or perhaps vapor deposition. Rock weathering is dominated by preferential destruction of olivine, as appropriate for acidic conditions.

[38] 2. Rocks encountered in the Columbia Hills up to and including exposures along the Cumberland Ridge are layered, granular deposits with bedding or exfoliation surfaces that tend to be conformable with topography. The rocks are enriched in alteration phases, including goethite, hematite, and nanophase iron oxides, relative to plains rocks. Some of the rocks exhibit a form of cavernous weathering indicative of differential cementation associated with aqueous fluid-rock interactions. The leading hypothesis is that the Hills rocks are thought to have been emplaced as volcaniclastic deposits and/or by impact ejecta emplacement (suggested by high nickel content for West Spur rocks) processes. The presence of aqueous acid-sulfate conditions during and/or after emplacement best explains rock alteration properties.

[39] 3. Soils in the plains and Columbia Hills are similar to the plains olivine-bearing basalts, implying that wind and perhaps impact processes have homogenized these deposits at least over the length scale of several kilometers traversed by Spirit. The addition of aqueous phases, including magnesium sulfates for The Boroughs Trench in the plains, and magnesium and iron sulfates for the Paso Robles deposit on Husband Hill, is required to explain observed elemental and chemical trends.

[40]   4. The landing site and surroundings are in an active aeolian environment, perhaps enhanced by mesoscale winds associated with the topography of Gusev Crater and by the superadiabatic temperature profiles that dominate the day time atmosphere. Active dust devils, wind-induced erosion of soil accumulated on the solar panels, and examination of soil surfaces and how they change due to high winds all point to continuing aeolian activity. Yet, the presence of equally spaced clasts and surface deposits of coarse sand grains suggests that significant erosion and redistribution happens only rarely in the current environment or that these coarse-grained materials were emplaced during an earlier period with a higher atmospheric density.

References

Alexander, D. A., et al. (2006), Processing of Mars Exploration Rover imagery for science and operations planning, *J. Geophys. Res.*, doi:10.1029/2005JE002462, in press.

Arvidson, R. E., S. W. Squyres, E. T. Baumgartner, P. S. Schenker, C. S. Niebur, K. W. Larsen, F. P. Seelos IV, N. O. Snider, and B. L. Jolliff (2002), FIDO prototype Mars rover field trials, Black Rock Summit, Nevada, as test of the ability of robotic mobility systems to conduct field science, *J. Geophys. Res.*, *107*(E11), 8002, doi:10.1029/2000JE001464.

Arvidson, R. E., et al. (2004a), Localization and physical properties experiments conducted by Spirit at Gusev Crater, *Science*, *305*(5685), 821–824, doi:10.1126/science.1099922.

Arvidson, R. E., J. Bibring, F. Poulet, S. W. Squyres, M. Wolff, and R. Morris (2004b), Coordinated Mars Exploration Rover and Mars Express OMEGA observations over Meridiani Planum, *Eos Trans. AGU*, *85*(47), Fall Meet. Suppl., Abstract P24A-06.

Bell, J. F., III, et al. (2004), Pancam multispectral imaging results from the Spirit rover at Gusev Crater, *Science*, *305*(5685), 800–806, doi:10.1126/science.1100175.

Bell, J. F., III, J. Joseph, J. N. Sohl-Dickstein, H. M. Arneson, M. J. Johnson, M. T. Lemmon, and D. Savransky (2006), In-flight calibration and performance of the Mars Exploration Rover Panoramic Camera (Pancam) instruments, *J. Geophys. Res.*, *111*, E02S03, doi:10.1029/2005JE002444.

Bertelsen, P., et al. (2004), Magnetic properties experiments on the Mars Exploration Rover Spirit at Gusev Crater, *Science*, *305*, 827–829.

Cabrol, N. A., et al. (2006), Conditions for aqueous processes at Gusev crater along the Spirit traverse: Assessment of fluid circulation and storage potential using the Microscopic Imager, *J. Geophys. Res.*, doi:10.1029/2005JE002490, in press.

Christensen, P. R., et al. (2004), Initial results from the Mini-TES experiment in Gusev Crater from the Spirit rover, *Science*, *305*(5685), 837–842, doi:10.1126/science.1100564.

Crumpler, L. S., et al. (2005), Mars Exploration Rover geologic traverse by the Spirit rover in the plains of Gusev crater, Mars, *Geology*, *33*(10), 809–812, doi:10.1130/G21673.1.

Farrand, W. H., J. F. Bell III, J. R. Johnson, S. W. Squyres, J. Soderblom, and D. W. Ming (2006), Spectral variability among rocks in visible and near-infrared multispectral Pancam data collected at Gusev crater: Examinations using spectral mixture analysis and related techniques, *J. Geophys. Res.*, *111*, E02S15, doi:10.1029/2005JE002495.

Fergason, R. L., P. R. Christensen, J. Bell, M. P. Golombek, K. Herkenhoff, H. H. Kieffer, and R. Sullivan (2006), Physical properties of the Mars Exploration Rover landing sites as inferred from Mini-TES derived thermal inertia, *J. Geophys. Res.*, doi:10.1029/2005JE002583, in press.

Gellert, R., et al. (2004), Chemistry of rocks and soils in Gusev Crater from the Alpha Particle X-ray Spectrometer, *Science*, *305*(5685), 829–832, doi:10.1126/science.1099913.

Gellert, R., et al. (2006), Alpha Particle X-Ray Spectrometer (APXS): Results from Gusev crater and calibration report, *J. Geophys. Res.*, doi:10.1029/2005JE002555, in press.

Goetz, W., et al. (2005), Indication of drier periods on Mars from the chemistry and mineralogy of atmospheric dust, *Nature*, *436*(7047), 62–65, doi:10.1038/nature03807.

Golombek, M., et al. (2005), Assessment of Mars Exploration Rover landing site predictions, *Nature*, *436*(7047), 44–48, doi:10.1038/nature03600.

Golombek, M. P., et al. (2006), Geology of the Gusev cratered plains from the Spirit rover transverse, *J. Geophys. Res.*, doi:10.1029/2005JE002503, in press.

Grant, J. A., et al. (2004), Surficial deposits at Gusev Crater along Spirit rover traverses, *Science*, *305*(5685), 807–810, doi:10.1126/science.1099849.

Grant, J. A., et al. (2006), Crater gradation in Gusev crater and Meridiani Planum, Mars, *J. Geophys. Res.*, *111*, E02S08, doi:10.1029/2005JE002465.

Greeley, R., et al. (2006), Gusev crater: Wind-related features and processes observed by the Mars Exploration Rover Spirit, *J. Geophys. Res.*, *111*, E02S09, doi:10.1029/2005JE002491.

Haskin, L. A., et al. (2005), Water alteration of rocks and soils on Mars at the Spirit rover site in Gusev crater, *Nature*, *436*(7047), 66–69, doi:10.1038/nature03640.

Herkenhoff, K. E., et al. (2004), Textures of the soils and rocks at Gusev Crater from Spirit's Microscopic Imager, *Science*, *305*(5685), 824–826, doi:10.1126/science.1100015.

Herkenhoff, K. E., et al. (2006), Overview of the Microscopic Imager Investigation during Spirit's first 360 sols in Gusev crater, *J. Geophys. Res.*, doi:10.1029/2005JE002574, in press.

Hurowitz, J. A., S. M. McLennan, N. J. Tosca, D. W. Ming, and C. Schröder (2006), In situ and experimental evidence for acidic weathering of rocks and soils on Mars, *J. Geophys. Res.*, *111*, E02S19, doi:10.1029/2005JE002515.

Johnson, J. R., et al. (2006), Spectrophotometric properties of materials observed by Pancam on the Mars Exploration Rovers: 1. Spirit, *J. Geophys. Res.*, doi:10.1029/2005JE002494, in press.

Larsen, K. W., R. E. Arvidson, B. L. Jolliff, and B. C. Clark (2000), Correspondence and least squares analyses of soil and rock compositions for the Viking Lander 1 and Pathfinder landing sites, *J. Geophys. Res.*, *105*(E12), 29,207–29,221.

Lemmon, M. T., et al. (2004), Atmospheric Imaging Results from the Mars Exploration Rovers: Spirit and Opportunity, *Science*, *306*(5702), 1753–1756, doi:10.1126/science.1104474.

Li, R., et al. (2006), Spirit rover localization and topographic mapping at the landing site of Gusev crater, Mars, *J. Geophys. Res.*, doi:10.1029/2005JE002483, in press.

McSween, H. Y., et al. (2004), Basaltic rocks analyzed by the Spirit Rover in Gusev Crater, *Science*, *305*(5685), 842–845, doi:10.1126/science.1099851.

McSween, H. Y., et al. (2006), Characterization and petrologic interpretation of olivine-rich basalts at Gusev crater, Mars, *J. Geophys. Res.*, *111*, E02S10, doi:10.1029/2005JE002477.

Ming, D. W., et al. (2006), Geochemical and mineralogical indicators for aqueous processes in the Columbia Hills of Gusev crater, Mars, *J. Geophys. Res.*, doi:10.1029/2005JE002560, in press.

Morris, R. V., et al. (2004), Mineralogy at Gusev Crater from the Mössbauer Spectrometer on the Spirit Rover, *Science*, *305*(5685), 833–836, doi:10.1126/science.1100020.

Morris, R. V., et al. (2006), Mössbauer mineralogy of rock, soil, and dust at Gusev crater, Mars: Spirit's journey through weakly altered olivine basalt on the Plains and pervasively altered basalt in the Columbia Hills, *J. Geophys. Res.*, doi:10.1029/2005JE002584, in press.

Smith, M. D., et al. (2004), First Atmospheric Science Results from the Mars Exploration Rovers Mini-TES, *Science*, *306*(5702), 1750–1753, doi:10.1126/science.1104257.

Squyres, S. W., et al. (2003), Athena Mars rover science investigation, *J. Geophys. Res.*, *108*(E12), 8062, doi:10.1029/2003JE002121.

Squyres, S. W., et al. (2004a), The Spirit Rover's Athena Science Investigation at Gusev Crater, Mars, *Science*, *305*(5685), 794–799, doi:10.1126/science.1100194.

Squyres, S. W., et al. (2004b), The Opportunity Rover's Athena Science Investigation at Meridiani Planum, Mars, *Science*, *306*(5702), 1698–1703, doi:10.1126/science.1106171.

Squyres, S. W., et al. (2006), Rocks of the Columbia Hills, *J. Geophys. Res.*, doi:10.1029/2005JE002562, in press.

Wang, A., et al. (2006a), Sulfate deposition in subsurface regolith in Gusev Crater, Mars, *J. Geophys. Res.*, doi:10.1029/2005JE002513, in press.

Wang, A., et al. (2006b), Evidence of phyllosilicates in Wooly Patch, an altered rock encountered at West Spur, Columbia Hills, by the Spirit rover

in Gusev Crater, Mars, *J. Geophys. Res.*, doi:10.1029/2005JE002516, in press.

Ward, J. G., R. E. Arvidson, and M. Golombek (2005), The size-frequency and areal distribution of rock clasts at the Spirit landing site, Gusev Crater, Mars, *Geophys. Res. Lett.*, *32*, L11203, doi:10.1029/2005GL022705.

Wolff, M. J., J. F. Bell III, P. B. James, R. T. Clancy, and S. W. Lee (1999), Hubble Space Telescope observations of the Martian Aphelion cloud belt prior to the Pathfinder mission: Seasonal and interannual variations, *J. Geophys. Res.*, *104*, 9027–9042.

Yen, A. S., et al. (2005), An integrated view of the chemistry and mineralogy of Martian soils, *Nature*, *436*(7047), 49–54, doi:10.1038/nature03637.

————————

R. C. Anderson, D. Blaney, W. Folkner, M. Golombek, C. Leff, T. Parker, R. Rieder, and A. Yen, Jet Propulsion Laboratory, California Institute of Technology, Pasadena, CA 91109, USA.

R. E. Arvidson, E. Guinness, L. Haskin, A. Wang, and J. Ward, Department Earth and Planetary Sciences, Washington University, Campus Box 1169, One Brookings Drive, St. Louis, MO 63130, USA. (arvidson@wunder.wustl.edu)

J. F. Bell III, S. W. Squyres, and R. Sullivan, Department of Astronomy, Space Sciences Building, Cornell University, Ithaca, NY 14853, USA.

J. Brückner and H. Wänke, Max Planck Institut für Chemie, Kosmochemie, D-55020 Mainz, Germany.

N. A. Cabrol, NASA Ames/SETI Institute, Moffett Field, CA 94035, USA.

W. M. Calvin, Geological Sciences, University of Nevada, Reno, Reno, NV 89557, USA.

M. H. Carr, U.S. Geological Survey, Menlo Park, CA 94025, USA.

P. R. Christensen, J. Farmer, R. Greeley, J. W. Rice Jr., and S. D. Thompson, Department of Geological Sciences, Arizona State University, Tempe, AZ 85287, USA.

B. C. Clark, Lockheed Martin Corporation, Littleton, CO 80127, USA.

L. Crumpler, New Mexico Museum of Natural History and Science, Albuquerque, NM 87104, USA.

D. J. Des Marais and M. Sims, NASA Ames Research Center, Moffett Field, CA 94035, USA.

P. A. de Souza Jr., Companhia Vale do Rio Doce, 20030-900, Rio de Janeiro, RJ, Brazil.

C. d'Uston, Centre d'Etude Spatiale des Rayonnements, F-31028 Toulouse, France.

T. Economou, Enrico Fermi Institute, University of Chicago, Chicago, IL 60637, USA.

W. H. Farrand, Space Science Institute, Boulder, CO 80301, USA.

S. Gorevan, Honeybee Robotics, New York, NY 10012, USA.

J. A. Grant, Center for Earth and Planetary Studies, Smithsonian Institution, Washington, DC 20560, USA.

J. Grotzinger, Massachusetts Institute of Technology, Earth, Atmosphere and Planetary Science, Cambridge, MA 02139, USA.

B. C. Hahn, J. A. Hurowitz, S. M. McLennan, and N. J. Tosca, Department of Geosciences, State University of New York, Stony Brook, NY 11794, USA.

K. E. Herkenhoff, J. R. Johnson, and L. A. Soderblom, U.S. Geological Survey, Flagstaff, AZ 86001, USA.

S. Hviid, Max Planck Institut für Sonnensystemforschung, Katlenburg-Lindau, Germany.

G. Klingelhöfer, D. S. Rodionov, and C. Schröder, Institut für Anorganische und Analytische Chemie, Johannes Gutenberg-Universität, D-55128 Mainz, Germany.

A. H. Knoll, Botanical Museum, Harvard University, Cambridge, MA 02138, USA.

G. Landis, NASA Glenn Research Center, Cleveland, OH 44135, USA.

M. Lemmon, Department of Atmospheric Sciences, Texas A&M University, College Station, TX 77843, USA.

R. Li, Department of Civil and Environmental Engineering and Geodetic Science, Ohio State University, Columbus, OH 43210, USA.

M. B. Madsen, Niels Bohr Institute, University of Copenhagen, DK-2100 Copenhagen, Denmark.

M. C. Malin, Malin Space Science Systems, San Diego, CA 92191, USA.

H. Y. McSween and J. Moersch, Department of Earth and Planetary Sciences, University of Tennessee, Knoxville, TN 37996, USA.

D. W. Ming and R. V. Morris, NASA Johnson Space Center, Houston, TX 77058, USA.

L. Richter, DLR Institute of Space Simulation, Cologne, Germany.

M. Smith, NASA Goddard Space Flight Center, Greenbelt, MD, USA.

P. Smith, Lunar and Planetary Laboratory, University of Arizona, Tucson, AZ, USA.

T. Wdowiak, Department of Physics, University of Alabama at Birmingham, Birmingham, AL, USA.

M. Wolff, Space Science Institute, Martinez, GA, USA.